Comparison of methods to estimate sediment flux in ancient sediment routing systems

*Christopher J. Brewer, Gary J. Hampson, Alexander C. Whittaker, Gareth G. Roberts, Stephen E. Watkins**

Department of Earth Science and Engineering, Imperial College London, London SW7 2AZ, United Kingdom.

**present address: Department of Earth Sciences, University of Geneva, 1205 Geneva, Switzerland.*

Abstract

The need to predict accurately the volume, timing and location of sediments that are transported from an erosional source region into a basin-depocentre sink is important for many aspects of pure and applied sedimentological research. In this study, the results of three widely used methods to estimate sediment flux in ancient sediment routing systems are compared, using rich input datasets from two systems (Eocene South Pyrenean Foreland Basin, Spain and late-Pleistocene-to-Holocene Gulf of Corinth Rift Basin, Greece) for which mapped, dated sediment volumes provide an independent reference value of sediment accumulation rates. The three methods are: (1) the empirical BQART model, which uses values of drainage basin area, relief, temperature, lithology and water discharge; (2) empirical scaling relationships between characteristic geomorphological parameters of sediment-routing-system segments; and (3) the “fulcrum” model, which uses the palaeohydrological parameters of trunk river channels to estimate downsystem sediment discharge. The BQART model and empirical geomorphological scaling relationships were originally developed using modern sediment routing systems, and have subsequently been applied to ancient systems. In contrast, the “fulcrum” model uses hydrological scaling relationships from modern systems, but was developed principally for application in ancient systems.

Our comparative analysis quantifies the sensitivity of the three methods to their input parameters, and identifies the data required to make plausible estimates of sediment flux for ancient sediment routing systems. All three methods can generate estimates of sediment flux that are comparable with each other, and are accurate to at least one order of

magnitude relative to independent reference values. The BQART model uses palaeoclimatic and palaeocatchment input data, which are accurate for sub-modern systems but may be highly uncertain in deep-time systems. Corresponding estimates of sediment flux are most sensitive to the accuracy with which the palaeocatchment area is constrained and to palaeoclimatic parameters that reflect temperature and precipitation. The "fulcrum" model uses palaeohydrological input data; its sediment-flux estimates are sensitive to palaeochannel dimensions and, in particular, the duration of bankfull discharge, which is invariably difficult to constrain accurately in deep-time sediment routing systems. This uncertainty can give rise to large potential ranges of sediment-flux estimates. Geomorphological scaling relationships offer comparable, order-of-magnitude accuracy for both sub-modern and deep-time sediment routing systems in which geomorphological segments can be identified, but when used on relatively small sediment routing systems the ranges of sediment volumes deposited can vary greatly, limiting the utility of the technique.

We suggest that methods to estimate sediment flux should be chosen for a particular sediment routing system based on the types and uncertainty of available data. Where input parameter values are highly uncertain, such as in deep-time systems, Monte Carlo simulation is an effective tool to calculate probability distributions of estimated sediment flux.

1. Introduction

Estimation of sediment flux is an important step in linking net-erosional source regions where sediment is generated, to net-depositional basin-depocentre sinks (Fig. 1A). In modern sediment routing systems, sediment flux can be measured at multiple locations, typically over short timescales (10^0-10^4 yr), and integrated to generate a sediment budget (e.g., Goodbred and Kuehl, 1999; Clift and Giosan, 2014). In ancient systems, sediment volumes can be mapped in appropriate chronostratigraphic context using outcrop and/or subsurface (e.g., seismic) data, and these volumes can then be used to calculate net-depositional sediment fluxes over long timescales (10^5-10^7 yr) (e.g., Liu and Galloway, 1997; Goodbred and Kuehl, 1999; Walford et al., 2005; Galloway et al., 2011; Clift and Giosan, 2014; Michael et al., 2014a, b; Hampson et al., 2014; Helland-Hansen et al., 2016; Watkins et al., 2019). Sediment volumes and accumulation rates in basin-depocentre sinks can be compared with eroded volumes and denudation rates in source regions to construct long-term sediment budgets (e.g. Rouby et al., 2009; Guillocheau et al., 2012). Such approaches can be used to constrain sediment supply controls (e.g., tectonic or climatic drivers) on stratigraphic architecture, lithology distribution and palaeogeography (e.g., Michael et al., 2014a, b), with potential application to the prediction of earth resources (e.g., as part of a source-to-sink approach to hydrocarbon exploration; Martinsen et al., 2010) and to the assessment of sedimentary archives of palaeoclimatic and tectonic change (e.g., Watkins et al., 2019; Fernandes et al., 2019; Lodhia et al., 2019). However, it is typically impossible to map in full the morphology of ancient source-region catchments and the volume of sediment deposited in associated depocentres, due to incomplete preservation and limited age constraints. Instead, proxy-based methods must be used to estimate sediment flux and sediment budgets in ancient sediment routing systems.

To date, three main methods have been used to estimate sediment flux over large spatial and temporal scales in ancient sediment routing systems: (1) The empirical BQART model, which uses values of drainage basin area, relief, temperature, lithology and water discharge to estimate suspended load sediment fluxes (Syvitski and Milliman, 2007) (Fig. 1B). This method was originally developed for modern systems, where it has been widely used, but has subsequently been adapted for application to ancient sediment routing systems (e.g., Eide et al., 2017; Liu et al., 2019). (2) Empirical scaling relationships between characteristic geomorphological parameters of sediment-routing-system segments, which have been developed for modern systems and have also been applied to seismically imaged ancient systems to constrain sediment fluxes (Sømme et al., 2009; Nyberg et al., 2018) (Fig. 1C). (3) The "fulcrum" model, which uses the palaeohydrological parameters of trunk river channels to estimate down-system sediment discharge (Holbrook and Wanas, 2014) (Fig. 1D). Each of these three methods is based on different assumptions and uses different input data to estimate sediment flux over the timescale of interest. However, it is currently unclear which of these methods, and in what circumstances, produce the most reliable estimates of time-integrated sediment supply, in comparison to independently mapped and dated sediment volumes.

The aims of this paper are threefold: (1) to review the three methods, listed above, that are currently used to estimate sediment flux in ancient sediment routing systems; (2) to compare the sediment-flux estimates generated by the three methods for two data-rich sediment routing systems; and (3) to use this comparison to establish recommendations for best-practice use of the three methods. The reference for comparison is provided by independent values of sediment accumulation rates calculated from mapped, dated sediment volumes of the two sediment routing systems selected as case studies. The first case study is of a deep-time sediment routing system, from Eocene strata of the South Pyrenean Foreland Basin, Spain, which has been characterised quantitatively using outcrop data (Michael et al., 2013, 2014a, b). The second case study is of an array of sub-modern, late-Pleistocene-to-Holocene sediment routing systems that supplied sediment to the Gulf of Corinth Rift Basin, Greece, which have been characterised quantitatively using a combination of seismic mapping in the depositional sink and geomorphological mapping of source catchments (Watkins, et al. 2019, 2020). The use of palaeo-sediment routing systems of different ages as case studies allows the effects of different input data types, distributions and resolutions on the sediment-flux estimation methods to be assessed.

2. Sediment-flux estimation methods

In the following section, we summarise briefly the three methods that are increasingly being used to estimate sediment flux in sediment routing systems. Figure 1B-D and Table 1 present the parameters for which input data are required for each method, and introduces the symbols that are used for these parameters throughout the paper. Three mechanisms of sediment transport are commonly considered when estimating sediment flux; bedload, suspended load, and dissolved load. The BQART model explicitly considers suspended load, while geomorphological scaling relationships and the “fulcrum” model consider both bedload and suspended load. Thus, dissolved load is not accounted for in any of the estimation methods considered herein. Globally, the dissolved load of rivers is approximately one quarter of the suspended load, and bedload is smaller still (e.g., Milliman and Meade, 1983; Meybeck, 1987).

2.1. BQART model

Estimation of sediment fluxes from terrestrial sources was initially approached by Syvitski et al. (2003) as the ART model (where A = catchment drainage area; R = catchment relief; T = catchment-averaged temperature), which then evolved into the BQART model (Q = water discharge; B = anthropogenic, glacial and lithological contribution) (Syvitski and Milliman, 2007). The BQART model is empirical and uses topographic and climatic characteristics of the catchment area, which can be measured directly in modern systems, as input data (Fig. 1B). By parameterising the BQART model using a global database of the suspended load of 488 modern river systems, Syvitski and Milliman (2007) established that it can account for 96% of data variance in the short-term record (10^0-10^1 yr) contained in the database. The BQART model predicts average suspended sediment load, Q_s (in units of Mt/yr) as:

$$Q_s = \omega B Q_w^{0.31} A^{0.5} R T \text{ for } T \geq 2^\circ\text{C} \quad (1a)$$

$$Q_s = 2\omega B Q_w^{0.31} A^{0.5} R \text{ for } T < 2^\circ\text{C} \quad (1b)$$

where ω is a constant, 0.0006 (giving Q_s in units of Mt/yr), Q_w is water discharge (in units of km^3/yr), A is catchment drainage area (in units of km^2), R is maximum catchment relief (in units of km), T is long-term catchment-averaged temperature (in units of ˚C), and B is defined by:

$$B = IL(1-T_E)E_h \quad (2)$$

where I is a glacial erosion factor (≥1), L is a catchment-averaged lithology factor, T_E is the trapping efficiency of lakes and reservoirs (≤1), and E_h is a human-influenced soil erosion factor (Syvitski and Milliman, 2007). In modern sediment routing systems, B can be estimated for individual catchments (e.g., Table 7.1 in Allen, 2017) or as a global average (e.g., Table A41.1 in Allen and Allen, 2013). It is reasonable to assign a value of B = 1 in applications of the BQART model to non-glaciated catchments in deep-time systems, as in our case-study analysis of two sediment routing systems below, given the lack of glacial erosion (I = 1); the global mean value of lithology factor (L = 1; Syvitski and Milliman, 2007); the low degree of sediment trapping in catchments not influenced by human activity (T_E = 0); the absence of human influence (E_h = 1); and to avoid a potentially arbitrary assignment of differing L values at the catchment level. In modern systems for which detailed calculation is possible, values of B vary between 0.3 and 7 (e.g., Kettner et al., 2010; Restrepo et al., 2015); however, the BQART model still accounts for 68% of the variation in sediment load between modern rivers using a value of $B = 1$ (Syvitski and Milliman, 2007).

The accuracy of the BQART model has been demonstrated in specific modern systems, based on comparison of its sediment-flux predictions with the values of time-averaged sediment flux derived from water balance models and high-resolution digital elevation models, in conjunction with measured sediment concentrations (e.g., Liquete et al., 2009; Kettner et al., 2010). The BQART model has also been applied to ancient sediment routing systems (e.g., Weight et al., 2011; Allen et al., 2013; Sømme et al., 2013; Zhang et al., 2018). In these deep-time applications of the BQART model, A is constrained by sedimentary provenance analysis, plate tectonic reconstructions, and geomorphological analyses. R can be estimated using structural restoration, thermochronology, palaeobotanical data, numerical modelling of landscape evolution, paleoaltimetry, and tectonic analogues. T can be estimated using oxygen isotope geochemistry, palaeontological data, palaeosol analysis, and palaeoclimate models. Q_w (in units of m^3/s) can be estimated using an empirical relationship with A (in units of km^2) derived by Milliman and Syvitski (2007) for their database of modern rivers:

$$Q_w = 0.075\, A^{0.8} \qquad (3)$$

However, estimates of Q_w can also be refined by accounting for precipitation variations across palaeoclimate zones (Davidson and North, 2009; Eide et al., 2018). B is either equal to 1 (e.g., Allen et al., 2013) or is calculated using appropriate values of I, L and T_E that account for glacial erosion, catchment lithology, and sediment trapping efficiency for a particular ancient sediment routing system (e.g., Zhang et al., 2018). In our analyses below, we report values of sediment flux derived using the BQART model in units of km^3/Myr.

An obvious uncertainty in applying the BQART model to ancient sediment routing systems is that it only accounts for suspended sediment load (Syvitski and Milliman, 2007), and does not include bedload. Sediment flux may therefore be systematically underestimated. In addition, the influence of high-amplitude, low-frequency discharge events, which are infrequently sampled by the recent data used to develop the model, may be underestimated. More speculatively, soil erosion, which is represented by the value of E_h, may have varied in deep time due to evolution of vegetation and grazing fauna, rather than human influence (e.g., Gibling et al., 2012).

2.2. Geomorphological scaling relationships

Empirical scaling relationships between the dimensions of four geomorphological segments (catchment, shelf, slope, basin floor) of sediment routing systems (Fig. 1C) were first developed by Sømme et al. (2009) using data from 29 modern continental-margin systems, and then refined by Nyberg et al. (2018) using an expanded database of 69,586 modern systems that are also predominantly from continental margins. Their analyses derived empirical scaling relationships, with the form of a power law, between parameters that describe the dimensions of different segments (Sømme et al., 2009; Nyberg et al., 2018). Many of the scaling relationships are similar for both the smaller, older dataset and the larger, newer dataset (Nyberg et al., 2018). The segment-based method allows the morphological parameters of up-system segments (e.g., catchment) to be linked to the morphological parameters of down-system segments (e.g., basin-floor fan), and vice versa. The up-system segments of ancient sediment routing systems are typically poorly preserved, and this method allows their dimensions and morphology to be estimated from the geometrical characteristics of down-system segments.

In the two case studies presented below, we use two of the geomorphological scaling relationships presented by Sømme et al. (2009) to estimate basin-floor fan volumes: (1) length of main (trunk) river channel vs. slope length; and (2) slope length vs. basin-floor fan volume. Nyberg et al. (2018) caution against using slope length as a parameter in geomorphological scaling relationships, because the limits of the slope segment are difficult to define in modern sediment routing systems in their expanded dataset, and because slope morphology likely reflects multiple, potentially interacting sedimentological and tectonic controls. Despite these caveats, we have used the relationships of Sømme et al. (2009), which are valid for their smaller dataset. Basin-floor fan volumes could alternatively be estimated using different data inputs (e.g., catchment drainage area, *A*, and fluvial-palaeochannel slope, *S*; Table 1) and combinations of scaling relationships. However, these alternative methods would use a larger number of scaling relationships to estimate basin-floor fan volume, long-term fan deposition rate, or riverine sediment load in the two case studies presented below, and thus lead to an increased range of uncertainty.

Our approach also uses basin-floor fan volume in the passive-margin systems considered by Sømme et al. (2009) as a proxy for the sediment volume deposited by the sediment routing system. In many sediment routing systems, sediment is sequestered either temporarily or permanently in geomorphological segments up-system of the basin floor (e.g., Hinderer, 2012). Temporary storage of sediment in up-system segments reflects intermittent, short-term availability of accommodation (e.g., on the shelf during relative sea-level highstands), and such sediment may be deposited ultimately on the basin floor if sufficiently long timescales (e.g., one or more complete relative sea-level cycles) are considered (e.g., Blum et al., 2009; Hinderer, 2012). Permanent storage of sediment in up-system segments occurs where tectonically subsiding depocentres are located in those up-system locations (e.g., Strong et al., 2005; Hinderer, 2012; Paola and Martin, 2012). The sediment routing systems in both case studies presented below are associated with permanent storage of sediment before the basin floor (e.g., in alluvial, fluvial, deltaic, and/or slope deposits), and these deposits are therefore included in our estimates of sediment volume. The sediment volume deposited by the sediment routing system (as approximated by basin-floor fan volume in the geomorphological scaling relationships of Sømme et al., 2009) is then divided by the duration of deposition to estimate net-depositional sediment flux. Since the geomorphological scaling relationships have been derived from modern systems, we assume that the sediment volume and related net-depositional sediment flux do not include significant compactional effects (i.e. they are decompacted).

Although the scaling methodology is powerful in allowing predictions based on scaling between different segments of the sediment routing system, and it can be applied to ancient systems whose morphology is imaged in seismic data (e.g., Sømme et al., 2013), the scatter of data around each scaling relationship is large. Additional uncertainty is introduced by the use in our analysis of slope length as a scaling parameter, and of basin-floor fan volume as a proxy for sediment volume. The resulting uncertainty is such that geomorphological parameters can be predicted only within one-to-three orders of magnitude.

2.3. "Fulcrum" model

The "fulcrum" model uses the palaeohydrological parameters of trunk-river channels to estimate downsystem sediment flux in ancient sediment routing systems, by assuming that the sediment mass transported through a cross-section of the trunk channel (i.e. the "fulcrum") is balanced by the sediment mass eroded upsystem and deposited downsystem (Holbrook and Wanas, 2014) (Fig. 1D). The model relies on preservation of the trunk-river palaeochannel, which links the up-system catchment segment to the down-system slope and basin-floor segments. The position and dimensions of the trunk-river palaeochannel are assumed to be fixed during the period over which sediment flux is estimated.

The first step in applying the "fulcrum" model is to estimate the wetted perimeter of the trunk-river palaeochannel, and to sample representatively its bedload grain size (Holbrook and Wanas, 2014). Typically, palaeochannel wetted perimeter is estimated as the product of averaged bankfull depth, H_{bf}, and bankfull width, B_{bf}, which assumes a rectangular palaeochannel (Holbrook and Wanas, 2014), although it can be measured directly in modern channels and well-preserved palaeochannels. Palaeochannel depth can be approximated from the measured thickness of a palaeochannel-fill storey (e.g., using the criteria of Bridge and Tye, 2000), which is then decompacted (e.g., Ethridge and Schumm, 1978), or estimated from cross-set thickness (e.g., Leclair and Bridge, 2001; Ganti et al., 2019), although it should be noted that the averaged bankfull depth of a palaeochannel is smaller than its thalweg depth. Palaeochannel width can be either directly measured, if data are available (e.g., at outcrop), or estimated using one or more empirical relationships linking channel depth and width in modern rivers (e.g., Bridge and Mackey, 1993). Some combinations of bankfull palaeochannel width (B_{bf}) and averaged bankfull depth (H_{bf}) are inconsistent with input data. To identify such combinations, and remove them from our analysis, we estimate palaeochannel hydraulic radius, R_{bf}, and use it as a filtering parameter:

$$R_{bf} = (B_{bf} H_{bf})/(B_{bf} + 2H_{bf}) \quad (4)$$

Median bedload grain size, D_{50}, can be approximated by the grain size of dune-scale cross-bed sets in the lower part of a palaeochannel-fill storey (Holbrook and Wanas, 2014).

The second step is to estimate bankfull discharge of water and sediment through the palaeochannel (Holbrook and Wanas, 2014). This requires estimation of palaeochannel slope, S. Channel slope can be measured directly in modern channels, or estimated, as in the original version of the fulcrum approach, by:

$$\tau^*_{bf50} = (H_{bf}\, S)/(\rho_{s\text{-}w}\, D_{50}) \qquad (5)$$

where τ^*_{bf50} is the bankfull Shields stress (dimensionless shear stress) for the entrainment of sand or granules (which is taken to be 1.86 after Parker, 1978) at median grain size and $\rho_{s\text{-}w}$ is the dimensionless value of submerged density of bedload sediment grains:

$$\rho_{s\text{-}w} = (\rho_s / \rho_w) - 1 \qquad (6)$$

where ρ_s is the density of bedload sediment grains and ρ_w is the density of water. $\rho_{s\text{-}w}$ has a value of 1.65 for quartz. While gravel bed rivers have Shields stresses which are typically of the order of 0.06, and suspension dominated systems have Shields stresses of the order of 10, the use of τ^*_{bf50} ~ 2 would be consistent with mixed load systems (Dade and Friend, 1998). Channel bankfull discharge, Q_{bf}, is estimated using:

$$C_f\, [(Q_{bf}^{2})/(B_{bf}^{2}\, H_{bf}^{2})] = g\, H_{bf}\, S \qquad (7)$$

$$C_f^{-1/2} = 8.32\, (H_{bf}^{2} / k_s) \qquad (8)$$

where C_f is the dimensionless Chezy friction coefficient, and $k_s = H_{bf}/8$ (after Leclair and Bridge, 2001). Bankfull discharge of suspended load is estimated according to the method of Van Rijn (1984). Consequently, total bedload discharge, Q_{tdf}, is estimated as:

$$Q_{tdf} = B_{bf}\, (\rho_{s\text{-}w}\, g\, D_{50})^{1/2}\, D_{50}\, \alpha_t\, (\varphi_s\, \tau^*_{bf50} - \tau^*_c)^{nt} \qquad (9)$$

where g is the acceleration due to gravity (9.81 ms^{-1}) and, from the estimation of Engelund and Hansen (1967) for sand-bed rivers, $\alpha_t = \alpha_{EH}/C_f$, $\alpha_{EH} = 0.05$, $n_t = 2.5$, $\varphi_s = 1$, $\tau^*_c = 0$. Finally, the total mean annual sediment volume discharged through the channel, Q_{mas}, is given by (Holbrook and Wanas, 2014):

$$Q_{mas} = Q_{bts}\, (t_{bd})\, b \qquad (10)$$

where Q_{bts} is the average total bankfull sediment discharge rate (combining bedload discharge, Q_{tdf}, and suspended load), t_{bd} is the year-averaged bankfull duration, and b is a dimensionless multiplier expressing the inverse of the proportion of the total annual sediment load carried over the year-averaged bankfull duration – this can also be referred to as the intermittency of sediment transport (e.g., Parker et al., 1998; Singh et al., 2009). It is important to note that there is wide variability in the proportion of time for which rivers are at bankfull discharge in modern systems, which is when the majority of sediment transport is assumed to occur (e.g., Meybeck et al., 2003), but a value of 2% (i.e., 7.3 days per year) is taken to be a default value for t_{bd} in the original form of the fulcrum approach (Holbrook and Wanas, 2014). The calculated value of Q_{mas} represents the annual mean sediment flux through the trunk-river palaeochannel, and is multiplied by the duration of the time interval under investigation to give the volume of sediment transported through the palaeochannel.

In principle, the "fulcrum" model allows the use of sparse, high-resolution datasets that intersect trunk-river palaeochannels and sample representatively their palaeohydrological archive (e.g., core or outcrop data through a palaeochannel axis) to reconstruct sediment flux. There are multiple sources of potential error and uncertainty in each step of applying the "fulcrum" model to ancient sediment routing systems, including misidentification of the trunk river palaeochannel, incorrect measurement of palaeochannel dimensions (H_{bf}, B_{bf}) due to incomplete preservation, approximations in each of the palaeohydraulic and sediment transport equations (which become compounded as multiple equations are used), and underestimation or overestimation of year-averaged bankfull duration (t_{bd}). To date, this method has been tested on three ancient sediment routing systems: the outcropping Cretaceous Bahariya Formation, Egypt (Holbrook and Wanas, 2014) and Cretaceous Ferron Sandstone, USA (Sharma et al., 2017), and the Cretaceous Dunvegan Formation, Canada, using a combination of well-log, core and outcrop data (Lin and Bhattacharya, 2017). In these cases, comparison with mapped sediment volumes in down-system locations suggests that the "fulcrum" model generated a robust order-of-magnitude estimate of sediment flux. In our analyses below, we report values of sediment flux derived using the "fulcrum" model in units of km^3/Myr.

2.4. Errors and uncertainty

As outlined above, each of the three sediment flux estimation methods has multiple sources of error, arising from measurement accuracy, and uncertainty, arising from the use of sparse data distributions. Three approaches have been taken to characterise error and uncertainty in using the different estimation methods.

Where mathematical models between input and output parameters are simple, such as in the power-law geomorphological scaling relationships of Sømme et al. (2009) and Nyberg et al. (2018), then uncertainty can be propagated using an appropriate mathematical relationship. In our analysis, we use the graphical expression of the geomorphological scaling relationships presented by Sømme et al. (2009) for: (1) length of main (trunk) river channel vs. slope length; and (2) slope length vs. basin-floor fan volume to estimate basin-floor fan volume as a proxy for sediment volume, which is equivalent to multiplying the fractional uncertainty in the length of the trunk river channel by the product of the two power-law coefficients. The best-fit trendlines for graphs of the scaling relationships (from figure 15 of Sømme et al., 2009) were used to derive most likely estimates of, first, slope length and then, second, basin-floor fan volume. Trendlines defining the 90% confidence envelope for each scaling relationship (from figure 15 of Sømme et al., 2009) were used to derive minimum and maximum estimates of slope length and thus basin-floor fan volume, to define uncertainty in the predicted volumes. The resulting uncertainty is large, because the 90% confidence envelope for each scaling relationship encompasses one-to-three orders of magnitude, and because the range of uncertainty in basin-floor fan volume has been propagated from two scaling relationships. The resulting estimates of basin-floor fan volume have been divided by a single value for the duration of deposition of the sediment routing system, which does not account for uncertainty in age dating, to give estimates of net-depositional sediment flux.

Where mathematical models between input and output parameters are complicated and there is large uncertainty in the input parameters, such as in deep-time applications of the BQART or “fulcrum” models, then Monte Carlo simulation is appropriate for uncertainty propagation (e.g., Hammersley and Handscombe, 1964), as demonstrated elegantly for the BQART model by Zhang et al. (2018). Ranges and an associated distribution of values for each input parameter in the BQART or “fulcrum” models (e.g., rectangular, triangular, normal, log normal) were chosen for the parameter values, to quantify uncertainty in input parameters, and then uncertainties were propagated using Monte Carlo simulation. This resulted in probability distribution outputs of estimated sediment flux. It is assumed that there is no uncertainty in the formulation of the BQART or "fulcrum" models, such that the multipliers and power law coefficients assigned to input parameters are held constant in the Monte Carlo simulation. For example, constant values of the multiplier (ω) and power law coefficients assigned to Q_w (0.31), A (0.5), B, R, and T (1) are used in our Monte Carlo simulation of the BQART model. A sufficiently large number of simulated samples, or trials (10,000 runs, as per convention, in our analysis), must be generated to assess uncertainty in sediment flux.

Where a probabilistic approach to sediment-flux estimation is inappropriate, because there is negligible measurement error and input parameters do not exhibit continuous distributions, then it may be appropriate to develop multiple deterministic scenarios to characterise uncertainty. Watkins et al. (2019) used a scenario-based approach in their application of the BQART model to sub-modern sediment routing systems, in which catchment characteristics were subject to negligible measurement error and a small number of discrete age models (with corresponding climate characteristics) was considered. Below, we adopt a similar scenario-based approach to applying the "fulcrum" model to the same sub-modern sediment routing systems, since input hydrological parameters have little measurement error (e.g. channel wetted perimeter).

3. Application to Eocene sediment routing system of the South Pyrenean Foreland Basin

3.1. Geological setting

The first sediment routing system investigated in this study – the Escanilla sediment routing system – is upper Eocene in age, and developed in the wedge top of the South Pyrenean Foreland Basin system, in the present-day Tremp-Graus, Ainsa, and Jaca basins (Fig. 2) (e.g. Michael et al., 2013; Allen et al., 2013). Provenance analyses and geologic mapping show that the upstream source catchments of the sediment routing system lay in the Pyrenean Axial Zone, from which sediment was routed southward through the Gurb-Pobla, Sis and

Santa Orasia palaeovalleys into the west-to-east-trending wedge top (Michael et al., 2014b) (Fig. 2). From east (up-system) to west (down-system), the deposits of the sediment routing system comprise: (1) alluvial conglomerates in the palaeovalley fills; (2) fluvial gravels, sandstones, siltstones and mudstones in the Tremp-Graus and Ainsa basins; and (3) deltaic, slope and basin-floor sandstones, siltstones and mudstones in the Jaca Basin. The footprint or "fairway" of the Escanilla sediment routing system has been reconstructed via integration of a range of methods, including detailed mapping, sedimentological logging, sedimentary provenance analysis, biostratigraphic correlation, thermochronological data, and analysis of grain-size patterns, using extensive exposures of late Eocene strata in the Southern Pyrenees (Whitchurch et al., 2011; Whittaker et al., 2011; Parsons et al., 2012; Michael et al., 2013, 2014a, b; Armitage et al., 2015).

Michael et al. (2014a, b) identified three time intervals within the Escanilla sediment routing system (Escanilla Formation and time-equivalent strata). The upper part of the system was the most areally extensive and was deposited in a 2.6 Myr period, from 36.5 to 33.9 Ma (interval 3 of Michael et al., 2013, 2014a, b), based on biostratigraphic and magnetostratigraphic data with a temporal resolution of 0.5 Myr. This latter time interval is the one considered in our analysis below. Palaeocatchment area, *A*, and relief, *R*, are estimated to be between 4,000-19,000 km^2 and 1-5 km, respectively (Table 2), based on sedimentary provenance analysis, regional bedrock mapping, and exhumation rates constrained by fission track analysis (Michael et al., 2014a). The length of the Escanilla trunk-river palaeochannel is estimated at 80-140 km (Table 2), from mapping of the sediment routing system "fairway" (Michael et al. (2013, 2014b). Channelized fluvial sandbody widths and thicknesses have been measured using geo-referenced LIDAR and high-resolution photographic data, supplemented by direct field measurements, in the southern part of the Ainsa Basin (Fig. 2) (Labourdette, 2011). The internal architecture of the channelized sandbodies indicates that they generally record deposition from multiple-thread, braided-rivers, in which multiple channels were active at the same time (Dreyer et al., 1993; Labourdette, 2011). Palaeochannel-fill storeys comprise mainly coarse- to medium-grained, cross-bedded sandstones, which overlie basal gravels (Labourdette, 2011). Palaeoclimate is reconstructed to have been warm, dry and seasonal, using a combination of palaeobotanical data, oxygen isotope proxies, and climate model predictions (Cavagnetto and Anadon, 1996; Zachos et al., 2001, 2008; Scheibner et al., 2007; Pound and Salzmann, 2016; Inglis, et al. 2017).

Michael et al. (2014a) calculated the volume of the Escanilla sediment routing system deposits in the interval of interest (their interval 3) to be 1750 ± 157 km^3 after burial and compaction. The uncertainty in this volumetric estimate accounts for projection of sediment volumes between mapped outcrops. Given the estimated 2.6 Myr duration of this interval, the estimated accumulation rate of compacted sediment is 682 ± 61 km^3/Myr (Michael et al., 2013, 2014b). An additional volume of c. 80 km^3 is estimated to have been removed by localised erosion at the overlying base-Oligocene unconformity; incorporating this volume results in an estimated value of 713 ± 61 km^3/Myr for the accumulation rate of compacted sediment (Michael et al., 2014b). The reported sediment volumes and accumulation rates include an estimated average porosity of 13% (Michael et al., 2014a). Assuming an initial porosity at surface of 55% (e.g., Sclater and Christie, 1980; Watkins et al., 2019) gives a decompacted sediment accumulation rate of 1380 ± 118 km^3/Myr. The budget of the sediment routing system is not completely closed during the interval of interest, because the routing system "fairway" likely extends beyond the down-system (westward) limit of outcrop control (Michael et al., 2013, 2014a, b).

3.2. Application of BQART model

The value ranges and distributions of five input parameters (B, Q_w, A, R, and T) are estimated in applying the BQART model to estimate sediment flux in the Escanilla sediment routing system (Equation 1a; Table 2, based on published constraints outlined above). These distributions were then combined using Monte Carlo simulation.

Catchment area, A, is assigned a rectangular distribution with a range of 4,000-19,000 km^2 to indicate high uncertainty. The maximum catchment relief, R, is assigned a triangular distribution with the range 1-5 km and a mode of 2.5 km. The estimated range of catchment-averaged temperature, T, is 19-25 °C, and a triangular distribution is assigned with a mode of 22 °C. Water discharge, Q_w, is estimated to have a rectangular distribution with the range 1.0-6.4 km^3/Myr, using the empirical relationship between Q_w and A derived by Milliman and Syvitski (2007) (Equation 3). B represents the effects of anthropogenic, glacial and lithological influence on Q_s (Equation 2), and is assigned a value of 1. This is consistent with the lack of evidence for glacial erosion in the Axial Pyrenean Zone during the Eocene (i.e., I = 1), the evident absence of anthropogenic influence (i.e., E_h = 1, T_E = 0), and global compilations of catchment-averaged lithology factor (i.e., L = 1; cf. Table A41.1 in Allen and Allen, 2013). The globally averaged value of L = 1 is consistent with a mixture of hard and soft bedrock lithologies (Syvitski and Milliman, 2007).

3.3. Application of geomorphological scaling relationships

The Escanilla trunk river palaeochannel is assigned a length of 80-140 km (Table 2), which gives an estimated, decompacted terminal sediment volume of 146-2790 km^3. A single value of duration (2.6 Myr) was then used to calculate the range of sediment-flux estimates that correspond to this range of sediment volumes. The reported values of sediment-flux estimates form a triangular distribution with a modal value that represents a trunk-river channel length of 110 km, the best-fit trendline for trunk-river channel length vs. slope length, and the best-fit trendline for slope length vs. basin-floor fan volume. The minimum value of the triangular distribution represents a trunk-river channel length of 80 km, the lower 90%-confidence-envelope trendline for trunk-river channel length vs. slope length, and the lower 90%-confidence-envelope trendline for slope length vs. basin-floor fan volume. The maximum value of the triangular distribution represents a trunk-river channel length of 140 km, the upper 90%-confidence-envelope trendline for trunk-river channel length vs. slope length, and the upper 90%-confidence-envelope trendline for slope length vs. basin-floor fan volume.

3.4. Application of "fulcrum" model

We infer that the Escanilla sediment routing system was supplied by three trunk channels that drained the Gurb-Pobla, Sis and Santa Orasia catchments (Fig. 2). A cross-section through the trunk channel downstream of the confluence between the Gurb-Pobla and Sis tributaries was treated as the fulcrum, since the contribution from the Santa Orasia tributary was relatively small (c. 16% of sediment discharge; Michael at al., 2014b). We assume that the channelized fluvial sandbodies characterised by Labourdette (2011) are representative of the trunk palaeochannel downstream of this confluence. Values of palaeochannel bankfull width, B_{bf}, and averaged bankfull depth, H_{bf}, are taken to be identical to the widths and thicknesses of single-storey channel bodies and multilateral channel belts reported by Labourdette (2011). After decompacting by 8%, consistent with the clean, sandstone-dominated character of the palaeochannel fills (Scherer, 1987; Lander and Walderhaug, 1999), values of B_{bf} and H_{bf} are estimated to be 40-390 m and 3-20 m, respectively (Table 2), with modal values of 150 m and 10 m and with triangular distributions. Palaeochannel hydraulic radius, R_{bf}, is calculated for the single-storey channel bodies and multilateral channel belts reported by Labourdette (2011), with a range of 2.5-17.9 m and a triangular distribution (mode of 9.9 m). Median bedload grain size, D_{50}, is estimated to be 0.4-0.8 mm (Table 2) with a rectangular distribution, based on the descriptions of Labourdette (2011).

A range of estimated values for palaeochannel slope, S, is calculated using Equation (5), our estimated ranges of H_{bf} and D_{50}, and assuming a triangular distribution of values for submerged density of sediment grains, ρ_{s-w}, with a range of 1.60-1.70 and mode of 1.65, and bankfull Shields number for dimensionless shear stress, τ^*_{bf50} (1.86, after Parker, 1978) (Table 2). A range of estimated values for channel bankfull discharge, Q_{bf}, and bedload discharge, Q_{tdf}, is calculated using Equations (7), (8) and (9). We do not know the intermittency of sediment transport within the upper Eocence Escanilla formation, so we have used a triangular distribution of values for year-averaged duration of bankfull conditions, t_{bd}, with a range of 0.1-120 days and mode of 7.3 days (corresponding to the default value of Holbrook and Wanas, 2014) (Table 2). Using Equation (10) and the various parameter values above, the estimated range of total mean annual sediment volume discharged through the trunk-river palaeochannels, Q_{mas}, is calculated.

The parameters listed above, and summarised in Table 2, reflect uncertainty in the palaeohydraulic parameters used to estimate sediment flux in the “fulcrum” model. These parameter ranges and distributions were combined using Monte Carlo simulation to give a probability distribution of sediment-flux estimates (Fig. 4).

3.5. Results of sediment-flux estimation methods

The results of the three sediment-flux estimation methods and the independent reference value of sediment flux for the Escanilla Formation are displayed in Figure 5. All three methods generate ranges of sediment-flux estimates that are wide, over 1-3 orders of magnitude, but they do include the reference value. The geomorphological scaling relationships generate the smallest range of values (146-2790 km^3/Myr), and the median value (1100 km^3/Myr) gives the closest match to the reference value. The “BQART” and “fulcrum” models generate larger ranges of values (308-9050 km^3/Myr and 21-111,000 km^3/Myr, respectively), indicating greater uncertainty in the input parameters for these estimation methods, and have higher median values (1790 km^3/Myr and 11,600 km^3/Myr, respectively). Using only a single value for year-averaged duration of bankfull conditions, t_{bd}, of 7.3 days (i.e. the default value of Holbrook and Wanas, 2014) greatly reduces the range of values (114-8370 km^3/Myr) and median value (2330 km^3/Myr) generated by the “fulcrum” model.

The large ranges of predicted sediment-flux values for each estimation method are clearly due to the significant uncertainties in the input parameter values. For the geomorphological scaling relationships, this uncertainty is reflected in the large width of 90% confidence envelope surrounding the best-fit trendlines, which are propagated in our calculations. In our application of the “BQART” model, uncertainty principally resides in catchment area, A (51%), and catchment relief, R (33%), rather than palaeoclimatically controlled parameters Q_w (8%), which reflects precipitation, and T (7%) (Fig. 6). In our application of the “fulcrum” model, uncertainty in estimated sediment flux is principally associated with year-averaged bankfull duration, t_{bd} (56%), but there are significant contributions from bankfull palaeochannel width, B_{bf} (22%), and grain size, D_{50} (19%) (Fig. 7). Averaged bankfull palaeochannel depth, H_{bf}, palaeochannel hydraulic radius, R_{bf}, and submerged density of bedload grains, ρ_{s-w}, contribute little to uncertainty in sediment flux (2%, 1% and 0%, respectively (Fig. 7).

4. Application to late-Pleistocene-to-Holocene sediment routing systems of the Gulf of Corinth Rift Basin

4.1. Geological setting

The Gulf of Corinth Rift Basin is an active, asymmetrical, West-East-trending basin in southern central Greece that is undergoing rapid North-South-directed extension (5-15 mm/yr) (e.g., Bell et al., 2008; Taylor et al., 2011; Ford et al., 2013; Nixon et al., 2016) (Fig. 8). Basin rifting initiated in the early Pliocene, at <5 Ma (e.g., Ori, 1989; Ford et al., 2013; Nixon et al., 2016).The basin depocentre is occupied by the Gulf of Corinth, a nearly fully enclosed marine inlet of the Ionian Sea located between mainland Greece and the Peloponnese peninsula (Fig. 8). The Gulf of Corinth has a surface area of c. 2500 km^2, is 135 km long (West-East extent), is up to c. 30 km wide (North-South extent), and reaches a maximum depth of c. 860 m (Fig. 6) (Nixon et al., 2016). A large number of catchments (73 with area >5 km^2; Watkins et al., 2019, 2020) drain into the Gulf of Corinth depocentre. Effectively the Gulf represents a closed basin, bounded by the Rion sill at a water depth of 60 m at its western end during interglacials, and forming an isolated lake during glacial times (Nixon et al., 2016). The late Pleistocene (c. 130 ka) to Holocene sediment routing systems that supply the Gulf of Corinth depocentre have been characterised by Watkins et al., (2019) using geomorphological analysis of a 30-m-spatial-resolution Advanced Spaceborne Thermal Emission and Reflection Radiometer (ASTER) digital elevation model (DEM) and field mapping of their subaerial components (cf. catchment and shelf segments of Sømme et al., 2009), and high-resolution seismic mapping of their subaqueous components (cf. slope and basin-floor segments of Sømme et al., 2009). Seismic data do not fully cover the subaqueous shelf. The shelf sedgment was estimated to contain only a small proportion (c. 6%) of the total sediment volume via extrapolation of the seismically mapped Holocene isopach, and sediment volumes mapped for the slope and basin-floor segments were then scaled accordingly (Watkins et al,. (2019). The resulting analysis has constrained sediment volumes in the depocentre, and estimated sediment fluxes from the associated catchments using the BQART model (Watkins et al., 2019).

Based on seismic-stratigraphic mapping of the Gulf of Corinth depocentre, time-to-depth conversion of seismic-stratigraphic volumes, seismic-well ties to establish stratal ages, and decompaction using the porosity-depth relationships of Angevine et al. (1990) and Nixon et al. (2016), Watkins et al. (2019) calculated the decompacted sediment volumes supplied by all sediment routing systems during the Holocene (0-12 ka; time interval 1 of Watkins et al., 2019) and late Pleistocene (12-130 ka; time intervals 2 and 3 of Watkins et al., 2019) to be 16 and 114 km^3, respectively. Each volume is divided by the duration of the relevant time interval, to give sediment accumulation rates of 1330 km^3/Myr for 0-12 ka and 970 km^3/Myr for 12-130 ka.

4.2. Application of BQART model

Watkins et al. (2019) document in detail the application of the BQART model to late Pleistocene (c. 130 ka) to Holocene sediment routing systems in the Gulf of Corinth Rift Basin, via the use of three scenarios with different age models for mapped seismic-stratigraphic units. Subsequently, age data collected by International Ocean Drilling Programme (IODP) Expedition 318 (McNeill et al., 2019a, b) indicate that only scenario 1 of Watkins et al. (2019) remains valid, and only this scenario is considered below. Values for catchment drainage area, A, and maximum catchment relief, R, were measured from the high-resolution DEM for all 73 large catchments (area >5 km^2) that drain into the Gulf of Corinth Rift Basin. A and R were assumed to have remained identical to the present during the last 130 kyrs, except that the value of R was increased by 60 m during the Last Glacial Maximum (12-70 ka), when sea level fell below the Rion sill (Watkins et al., 2019)/ As these measurements of A and R are very well constrained and have little error, no uncertainty was assigned to them. Values of long-term catchment-averaged temperature, T, and water discharge, Q_w, were derived, respectively, from mean annual temperatures for the Gulf of Corinth Rift Basin and from mean annual precipitation for each catchment. Watkins et al. (2019) generated multiple estimated values of T and Q_w for different time intervals of the last 130 kyrs (their Table 2). For time interval 1 (Holocene, 0-12 ka), catchment-specific values of modern T and mean annual precipitation (544-880 mm/yr) were taken directly from the high-resolution WorldClim datasets for 1950-2000 (Hijmans et al., 2005). An uncertainty of 10% was applied to these values. For time interval 2 (12-115 ka), values of T and catchment-specific mean annual precipitation were estimated using combinations of three different global climate models for the Last Glacial Maximum (12-70 ka) and the WorldClim datasets (Watkins et al., 2019); the possibility that rainfall was reduced by 200 mm/yr was also modelled based on palynological studies that suggested drier conditions prevailed at some times during the last glacial cycle. For time interval 3 (115-130 ka), the value of T (15 ˚C) was modified from the World-Clim datasets to account for a possibly warmer climate than the current interglacial, and values of catchment-specific mean annual precipitation (544-880 mm/yr) were taken directly from the WorldClim datasets, assuming the Holocene is representative of the period (Watkins et al., 2019). B is assigned a value of 1, consistent with the absence of glacial erosion (i.e., I = 1), anthropogenic influence (i.e., E_h = 1, T_E = 0), and global compilations of catchment-averaged lithology factor (i.e., L = 1; cf. Table A41.1 in Allen and Allen, 2013). As noted previously, the globally averaged value of L = 1 is consistent with a mixture of hard and soft bedrock lithologies (Syvitiski and Milliman, 2007).

4.3. Application of geomorphological scaling relationships

The length of the trunk river channel in all 73 large catchments (area >5 km^2) was measured from the high-resolution DEM. These lengths range from 1.8 km to 38.6 km. All resulting estimates of terminal sediment volume have been divided by the duration of the time interval 0-130 ka to give a triangular distribution of net-depositional sediment-flux estimates for each sediment routing system. The modal value for each triangular distribution represents the trunk-river channel length of a specific catchment, the best-fit trendline for trunk-river channel length vs. slope length, and the best-fit trendline for slope length vs. basin-floor fan volume. All net-depositional sediment-flux estimates assume that all sediment eroded from the catchment was bypassed to the basin-floor fan.

4.4. Application of "fulcrum" model

The "fulcrum" model was applied to each of the 73 sediment routing systems with large catchments (area >5 km^2), using direct field measurements. Values of channel bankfull width, B_{bf}, and averaged bankfull depth, H_{bf}, (3.1-126.2 m and 0.5-2.7 m, respectively), channel wetted perimeter, channel slope, S, and median bedload grain size, D_{50}, (0.2-229 mm) were measured at the mouth of each catchment (Watkins et al., 2020). Channel bankfull discharge, Q_{bf}, is calculated for each catchment using Equations (7) and (8), and measurements of channel wetted perimeter and S. Total bedload discharge, Q_{tdf}, is estimated for each catchment using Equation (9), measurements of B_{bf} and D_{50}, assumed values of $\rho_{s\text{-}w}$ (1.65 for quartz) and τ^*_{bf50} (1.86, after Parker, 1978), and estimated values of other parameters for sand-bed rivers (α_{EH} = 0.05, n_t = 2.5, φ_s = 1, τ^*_c = 0; Engelund and Hansen, 1967). The year-averaged bankfull duration, t_{bd}, of all catchments is estimated to be 4 hours per year from the WorldClim datasets (Watkins, 2019). Using Equation (10) and the various parameter values derived as stated above, the estimated total mean annual sediment volume discharged through the trunk-river palaeochannel, Q_{mas}, is calculated for each catchment (Fig. 9, reported in km^3/Myr). Fewer than c. 10% of the catchments (7 of 73) supply c. 70% of the sediment flux to the Gulf of Corinth depocentre (Fig. 9). We assume that field measurements of B_{bf}, H_{bf}, channel wetted perimeter, S, and D_{50} are accurate and representative, and that they can be applied to all three time intervals of Watkins et al. (2019). There is negligible error arising from direct field measurements in our estimates of sediment flux generated by the "fulcrum" model, but we apply a standard uncertainty of 10% that is consistent with the uncertainty in Watkins et al.'s (2019) application of the BQART model.

4.5. Results of sediment flux estimation methods

The results of the three sediment flux estimation methods and the reference value of sediment flux are displayed in Figure 10. Corresponding sediment volumes are reported in Table 3, for time intervals 0-12 ka and 12-130 ka. The "BQART" model generates sediment flux values (1600-1950 km^3/Myr and 1340 km^3/Myr, respectively, for time intervals 0-12 ka and 12-130 ka) that are comparable to the reference values of sediment accumulation rate

(1330 and 970 km^3/Myr for time intervals 0-12 ka and 12-130 ka) (Watkins et al., 2019). The "fulcrum" model generates similar sediment flux values (730-890 km^3/Myr for time interval 0-130 ka). The hydraulic, topographic and climatic input parameters for both "BQART" and "fulcrum" models can be measured directly for each of the 72 sediment routing systems (Fig. 8), assuming that these are representative for the time interval of interest. The geomorphological scaling relationships generate much larger, but less certain, estimates (range of 150-8,060,000 km^3/Myr and median value of 12,100 km^3/Myr for time interval 0-130 ka). This distribution of values is undoubtedly too high, given the geological constraints on the actual depositional volumes. However, the sediment routing systems measured in the Gulf of Corinth Rift Basin are much smaller than those in the datasets of Sømme et al. (2009) and Nyberg et al. (2018), which focus on large systems developed at continental margins. Accordingly, the empirical scaling relationships may benefit from further calibration to small, climatically arid systems, such as those in the Gulf of Corinth Rift Basin.

5. Discussion

5.1. When is it appropriate to use each sediment flux estimation method?

Our analysis of the Escanilla and Gulf of Corinth sediment routing systems indicates that the BQART model, geomorphological scaling relationships and the "fulcrum" model are all capable of generating estimates of sediment fluxes for ancient sediment routing systems that are accurate, at least to one order of magnitude, compared to independent estimates of sediment accumulation rate derived from mapped, dated sediment volumes (Figs. 5, 10). The choice of method should therefore depend on the types of input data available and the uncertainty in these data, which will likely reflect the age and preservation of the sediment routing system being examined.

Where accurate palaeoclimatic and palaeotopographic data are available for individual or multiple catchments, then the BQART model is appropriate. This approach is relatively simple to apply and does not depend on a range of palaeohydraulic and sediment transport equations that may be difficult to calibrate from sparse outcrop or subsurface data.

However, the accuracy and availability of palaeoclimatic and palaeotopographic data is far greater for sub-modern systems (e.g., Gulf of Corinth sediment routing systems; Fig. 10), and the uncertainty associated with such data increases significantly for deep-time settings, for which palaeocatchment dimensions and relief may be difficult to estimate (e.g., Escanilla sediment routing system; Figs. 5, 6).

In cases where accurate palaeohydraulic data can be reliably reconstructed from outcrop studies for a trunk river(s) (e.g., Holbrook and Wanas, 2014; Sharma et al., 2017; Lin and Bhattacharya, 2017), then the “fulcrum” model is appropriate. In sub-modern sediment routing systems, identification of trunk-river channels is straightforward (e.g., Gulf of Corinth sediment routing systems; Fig. 8), but this may not be the case in deep-time sediment routing systems, particularly in the absence of extensive outcrop and 3D seismic data. However, our analysis of the Gulf of Corinth Rift Basin implies that, at the basin scale, it is sufficient to characterise the trunk rivers of the largest sediment routing systems, which account for most of the sediment flux (Fig. 9). The “fulcrum” model is particularly sensitive to uncertainty in the proportion of time for which rivers are at bankfull discharge (Fig. 7), which is poorly constrained in modern rivers (e.g., Meybeck et al., 2003) and even more uncertain in deep-time settings. This uncertainty could be reduced, to an extent, by consideration of catchment size and palaeoclimate, which both influence discharge variability (Meybeck et al., 2003).

Geomorphological scaling relationships offer comparable, order-of-magnitude accuracy for both sub-modern and deep-time sediment routing systems (e.g., Figs. 6, 8), provided that geomorphological segments can be identified effectively in available data. The accuracy of this method is determined by the large intrinsic uncertainty of the scaling relationships, which follow a power law and exhibit one-to-three orders of magnitude range between 90% confidence limits. This large uncertainty is a poor match to the high accuracy and extensive distribution of available data for many sub-modern sediment routing systems (e.g., Gulf of Corinth sediment routing systems; Fig. 10), but is likely to be more appropriate for their data-poor, deep time counterparts (e.g., Escanilla sediment routing system; Fig. 5). In deep-time systems, identification of geomorphological segments requires seismic and/or large-scale outcrop data, and the absence of major post-depositional structural deformation.

Where available data allow more than one of the three estimation methods to be applied, then estimates can be cross-checked against each other (e.g., Figs. 5, 10) to increase confidence in the results. Such cross-checking is valuable in mitigating the effect of errors and uncertainty specific to the BQART model, geomorphological scaling relationships and "fulcrum" model.

5.2. What are the key sensitivities for each sediment-flux estimation method?

In applying the BQART model to the catchments of sediment routing systems in deep time, when anthropogenic influence was absent, palaeoclimatic parameters related to temperature and precipitation (T, Q_w) provide one source of uncertainty; catchment palaeo-topography and area provide the other (A, R) (e.g., Fig. 6). Sediment flux estimates are linearly proportional to T and R, so these two parameters are particularly important. Catchment palaeo-topography can be constrained by a combination of sedimentary provenance, structural restoration, thermochronometric data that constrain spatio-temporal denudation variations, stable isotope data that constrain palaeoaltimetry, and tectonic analogues (e.g. Rowley and Garzione, 2007; Fan et al., 2014; Michael et al., 2014b). However, the catchments of deep-time sediment routing systems are only rarely preserved, and sediment-flux estimates may be highly sensitive to catchment palaeo-topographic parameters even in systems with robust geological constraints on A and R (e.g., Escanilla sediment routing system; Fig. 6). Palaeoclimate can be estimated using oxygen isotope geochemistry, palaeontology of flora and fauna, palaeopaedology, and palaeoclimate models (e.g., Hays and Grossman, 1991; Wolfe, 1995; Sheldon and Tabor, 2009). Both palaeoclimatic and catchment-palaeotopographic parameters can also be constrained to some extent by sedimentological facies-architectural analysis of outcrop data that aid screening for modern analogues (e.g., Davidson and North, 2009).

The "fulcrum" model is highly sensitive to year-averaged bankfull duration (t_{bd}), and to a lesser degree to palaeochannel dimensions (B_{bf}, H_{bf}) and bedload grain-size characteristics (D_{50}) (e.g., Fig. 7). Bedload grain size can be directly measured in outcrop and core, or estimated from wireline-log proxies such as porosity, and is thus likely to be relatively well constrained in both sub-modern and deep-time sediment routing systems. Palaeochannel dimensions can be reconstructed from sedimentological facies-architectural analysis of outcrop data, or approximated using core and wireline log data in combination with empirical relationships linking channel width and depth in modern rivers (e.g., Hampson et al. 2013), but with greater uncertainty in deep-time systems than in sub-modern systems. The duration of bankfull discharge, when most suspended load and bedload was transported, reflects palaeoclimate and palaeohydrology, and is far harder to constrain in deep time than palaeochannel dimensions and bedload grain size. This parameter also varies significantly in modern rivers, from a few hours per year in ephemeral rivers developed under arid and semi-arid climates (e.g., Gulf of Corinth; Watkins, 2019) to over 100 days per year in perennial rivers developed under humid climates (e.g., Mississippi River; LMRFC, 2019). These extreme values differ by up to three orders of magnitude from the default value of 7.3 days per year proposed by Holbrook and Wanas (2014). The duration of bankfull discharge therefore has a much greater impact on estimated sediment flux than palaeochannel depth, palaeochannel width or bedload grain size. For example, using the default value of 7.3 days per year for the Gulf of Corinth sediment routing systems, rather than the estimate of 4 hours per year from the WorldClim datasets (Watkins 2019), results in over a 40-fold increase in estimated sediment flux. Consideration of palaeoclimate may allow values of t_{bd} to be estimated with greater accuracy using modern analogues, rather than using the default value. Each of the input parameters for the "fulcrum" model (B_{bf}, H_{bf}, D_{50}, t_{bd}) may also vary through time, such that it may not be straightforward to establish average values of these parameters over the time scale of interest.

Geomorphological scaling relationships inherently carry large uncertainty, as reflected in their wide 90% confidence envelopes (Sømme et al., 2009; Nyberg et al., 2018). Such large uncertainty is appropriate in analysing poorly preserved deep-time sediment routing systems, but means that other methods are better equipped to provide accurate and reasonably constrained estimates of sediment flux in sub-modern systems that are rich in palaeoclimatic, palaeohydraulic and catchment-palaeotopographic data. As noted earlier in applying this estimation method to the Gulf of Corinth sediment routing systems, these scaling relationships could also potentially be further refined, thereby reducing uncertainty, by screening for system size, climate and tectonic setting (cf. Nyberg et al., 2018). For example, the tectonic setting, size and morphology of the small sediment routing systems in the Gulf of Corinth are very different from the large systems on passive margins from which the methodology was developed.

6. Conclusions

Three methods for estimating sediment flux are compared using data from the deep-time Escanilla sediment routing system (Eocene South Pyrenean Foreland Basin, Spain) and sub-modern Gulf of Corinth sediment routing systems (late-Pleistocene-to-Holocene Gulf of Corinth Rift Basin, Greece). The empirical BQART model uses input parameters linked to palaeoclimate and catchment palaeotopography to estimate suspended sediment flux. Empirical geomorphological scaling relationships between sediment routing system segments (catchment, shelf, slope, basin-floor fan) are used to estimate net-depositional sediment volumes and flux. The “fulcrum” model uses the palaeohydrological parameters of trunk river channels to estimate down-system sediment flux. Where input parameter values for a particular method are highly uncertain, Monte Carlo simulation can be used to calculate probability distributions of sediment flux. Where input parameter values are tightly constrained or exhibit discontinuous distributions, one or more deterministic scenarios can be used to generate sediment flux estimates.

All three methods can generate plausible ranges of estimated sediment flux that are comparable with each other, and are accurate to at least one order of magnitude relative to independent reference values of net-depositional sediment flux derived from mapped, dated sediment volumes in the studied sediment routing systems. Sediment flux estimates generated by the BQART model are most sensitive to catchment palaeotopographic parameters, which are tightly constrained in sub-modern systems but highly uncertain in deep-time systems, but they are also influenced by palaeoclimatic parameters. Sediment-flux estimates derived from geomorphological scaling relationships have significant inherent uncertainty, resulting in a broad distribution of values over one-to-three orders of magnitude, for both sub-modern and deep-time sediment routing systems. Sediment flux estimates generated using the “fulcrum” model are most sensitive to the duration of bankfull discharge, which is highly uncertain in deep-time systems, and to a lesser degree to trunk-river palaeochannel dimensions and bedload grain-size characteristics. The types of data available and uncertainty in these data should be used as the basis to select an appropriate estimation method(s), and multiple methods should be employed to check the plausibility of sediment flux estimates.

Acknowledgements

CJB acknowledges the support of a NERC Oil and Gas CDT PhD scholarship. SEW was funded by a NERC Science and Solutions for a Changing Planet DTP studentship and by an Imperial College Janet Watson Bursary. ACW was supported by Royal Society Research Grant RG140109 for work in the Gulf of Corinth. Oracle is thanked for the use of Crystal Ball software under academic licence for Monte Carlo simulation, and Schlumberger Limited for the use of Petrel software via an academic software donation for the interpretation of seismic data in the Gulf of Corinth. We are grateful for the constructive review and editorial comments of an anonymous reviewer, John Holbrook, Luca Caracciolo and Chris Fielding.

References

Allen, P.A., 2017. Sediment routing systems: the fate of sediment from source-to-sink. Cambridge University Press, Cambridge, UK, 407 p.

Allen, P.A., Heller, P.L., 2011. Dispersal and preservation of tectonically generated alluvial gravels in sedimentary basins. In: Busby, C., Perez, A.A. (Eds.), Tectonics of Sedimentary Basins: Recent Advances. Wiley-Blackwell, Chichester, UK, pp. 111-130.

Allen, P.A., Allen, J.R., 2013. Basin analysis: principles and applications to petroleum play assessment (3rd edition). Wiley-Blackwell, Chichester, UK, 619 p.

Allen, P.A., Armitage, J.J., Carter, A., Duller, R.A., Michael, N.A., Sinclair, H.D., Whitchurch, A.L., Whittaker, A.C., 2013. The Qs problem: Sediment volumetric balance of proximal foreland basin systems. Sedimentology 60, 102-130.

Angevine, C., Heller, P., Paola, C., 1990. Quantitative Sedimentary Basin Modeling. American Association of Petroleum Geologists, Continuing Education Course Notes 32, 132 p.

Armitage, J., Allen, P.A., Burgess, P.M., Hampson, G.J., Whittaker, A.C., Duller, R.A., Michael, N.A., 2015. Sediment transport model for the Eocene Escanilla sediment-routing system. Journal of Sedimentary Research 85, 1510-1524.

Bell, R.E., McNeill, L.C., Bull, J.M., Henstock, T.J., 2008. Evolution of the offshore western Gulf of Corinth. Geological Society of America Bulletin 120, 156-178.

Blum, M.D., Hattier-Womack, J., 2009. Climate change, sea-level change, and fluvial sediment supply to deepwater depositional systems. In: Kneller, B.C., Martinsen, O.J., McCaffrey, W.D. (Eds.), External Controls on Deep Water Depositional Systems, pp. 15-39 Society for Sedimentary Geology (SEPM), Special Publication 92.

Bridge, J.S., Mackey, S.D., 1993. A revised alluvial stratigraphy model. In: Marzo, M., Puigdefabregas, C. (Eds.), Alluvial sedimentation, pp. 317-336 International Association of Sedimentologists, Special Publication 17.

Bridge, J.S., Tye, R.S., 2000. Interpreting the dimensions of ancient fluvial channel bars, channels, and channel belts from wireline-logs and cores. American Association of Petroleum Geologists Bulletin 84, 1205-1228.

Cavagnetto, C., Anadón, P., 1996. Preliminary palynological data on floristic and climatic changes during the Middle Eocene-Early Oligocene of the eastern Ebro Basin, northeast Spain. Review of Palaeobotany and Palynology 92, 281-305.

Clift, P.D., Giosan, L., 2014. Sediment fluxes and buffering in the post-glacial Indus Basin. Basin Research 26, 369-386.

Dade, W.B., Friend, P.F., 1998. Grain-size, sediment-transport regime, and channel slope in alluvial rivers. The Journal of Geology 106, 661-676.

Davidson, S.K., North, C.P., 2009. Geomorphological regional curves for prediction of drainage area and screening modern analogues for rivers in the rock record. Journal of Sedimentary Research 79, 773-792.

Dreyer, T., Fält, L.M., Høy, T., Knarud, R., Steel, R.J., Cuevas, J.-L. 1993. Sedimentary Architecture of Field Analogues for Reservoir Information (SAFARI): a case study of the fluvial Escanilla Formation, Spanish Pyrenees. In: Flint, S.S., Bryant, I.D. (Eds.) The Geological Modelling of Hydrocarbon Reservoirs and Outcrop Analogues, pp. 57-80 International Association of Sedimentologists, Special Publication 15.

Eide, C.H., Klausen, T.G., Katkov, D., Suslova, A.A., Helland-Hansen, W., 2017. Linking an Early Triassic delta to antecedent topography: Source-to-sink study of the southwestern Barents Sea margin. Geological Society of America Bulletin 130, 263-283.

Eide, C. H., Muller, R., Helland-Hansen, W., 2018. Using climate to relate water discharge and area in modern and ancient catchments. Sedimentology 65, 1378-1389.

Engelund, F., Hansen, E., 1967. A monograph on sediment transport in alluvial streams. Technical University of Denmark 0stervoldgade 10, Copenhagen K.

Ethridge, F.G., Schumm, S.A., 1978. Reconstructing paleochannel morphologic and flow characteristics: methodology, limitations, and assessment. In: Miall, A.D. (Ed.) Fluvial Sedimentology, pp. 703-722 Canadian Society of Petroleum Geologists, Memoir 5.

Fan, M., Hough, B.G., Passey, B.H., 2014. Middle to late Cenozoic cooling and high topography in the central Rocky Mountains: constraints from clumped isotope geochemistry. Earth and Planetary Science Letters 408, 35-47.

Fernandes, V.M., Roberts, G.G., White, N.J., Whittaker, A.C., 2019. Continental-scale landscape evolution: a history of North American topography. Journal of Geophysical Research: Earth Surface 124, 2689-2722.

Ford, M., Rohais, S., Williams, E.A., Bourlange, S., Jousselin, D., Backert, N., Malartre, F., 2013. Tectono-sedimentary evolution of the western Corinth rift (Central Greece). Basin Research 25, 3-25.

Galloway, W.E., Whiteaker, T.L., Ganey-Curry, P., 2011. History of Cenozoic North American drainage basin evolution, sediment yield, and accumulation in the Gulf of Mexico basin. Geosphere 7, 938-973.

Ganti, V., Whittaker, A.C., Lamb, M.P., Fischer, W.W., 2019. Low-gradient, single-threaded rivers prior to greening of the continents. Proceedings of the National Academy of Sciences 116, 11652-11657.

Gibling, M.R., Davies, N.S., 2012. Palaeozoic landscapes shaped by plant evolution. Nature Geoscience 5, 99-105.

Goodbred Jr, S.L., Kuehl, S.A., 1999. Holocene and modern sediment budgets for the Ganges-Brahmaputra river system: Evidence for highstand dispersal to flood-plain, shelf, and deep-sea depocenters. Geology 27, 559-562.

Guillocheau, F., Rouby, D., Robin, C., Helm, C., Rolland, N., 2012. Quantification and causes of the terrigeneous sediment budget at the scale of a continental margin: a new method applied to the Namibia-South Africa margin. Basin Research 24, 3-30.

Hammersley, J.M., Handscomb, D.C., 1964. Monte Carlo methods. Methuen, London, 184 p.

Hampson, G.J., Jewell, T.O., Irfan, N., Gani, M.R., Bracken, B., 2013. Modest change in fluvial style with varying accommodation in regressive alluvial-to-coastal-plain wedge: Upper Cretaceous Blackhawk Formation, Wasatch Plateau, central Utah, USA. Journal of Sedimentary Research 83, 145-169.

Hampson, G.J., Duller, R.A., Petter, A.L., Robinson, R.A., Allen, P.A., 2014. Mass-balance constraints on stratigraphic interpretation of linked alluvial–coastal–shelfal deposits from source to sink: example from Cretaceous Western Interior Basin, Utah and Colorado, USA. Journal of Sedimentary Research 84, 935-960.

Hays, P.D., Grossman, E.L., 1991. Oxygen isotopes in meteoric calcite cements as indicators of continental paleoclimate. Geology 19, 441-444.

Helland-Hansen, W., Sømme, T., Martinsen, O., Lunt, I., Thurmond, J., 2016. Deciphering Earth's natural hourglasses: perspectives on source-to-sink analysis. Journal of Sedimentary Research 86, 1008-1033.

Hijmans, R.J., Cameron, S.E., Parra, J.L., Jones, P.G., Jarvis, A., 2005. Very high resolution interpolated climate surfaces for global land areas. International Journal of Climatology 25, 1965-1978.

Hinderer, M., 2012. From gullies to mountain belts: a review of sediment budgets at various scales. Sedimentary Geology 280, 21-59.

Holbrook, J. & Wanas, H., 2014. A fulcrum approach to assessing source-to-sink mass balance using channel paleohydrologic paramaters derivable from common fluvial data sets with an example from the Cretaceous of Egypt. Journal of Sedimentary Research 84, 349-372.

Inglis, G.N., Collinson, M.E., Riegel, W., Wilde, V., Farnsworth, A., Lunt, D.J., Valdes, P., Robson, B.E., Scott, A.C., Lenz, O.K., Naafs, B.D.A., 2017. Mid-latitude continental temperatures through the early Eocene in Western Europe. Earth and Planetary Science Letters 460, 86-96.

Kettner, A.J., Restrepo, J.D., Syvitski, J.P.M., 2010. A spatial simulation experiment to replicate fluvial sediment fluxes within the Magdalena River Basin, Colombia. Journal of Geology 118, 363-379.

Labourdette, R., 2011. Stratigraphy and static connectivity of braided fluvual deposits of the lower Escanilla Formation, South Central Pyrenees, Spain. American Association of Petroleum Geologists Bulletin 95, 585-617.

Lander, R.H., Walderhaug, O., 1999. Predicting porosity through simulating sandstone compaction and quartz cementation. American Association of Petroleum Geologists Bulletin 83, 433-449.

Leclair, S.F., Bridge, J.S., 2001. Quantitative interpretation of sedimentary structures formed by river dunes. Journal of Sedimentary Research 71, 713-716.

Lin, W., Bhattacharya, J.P., 2017. Estimation of source-to-sink mass balance by a fulcrum approach using channel paleohydrologic parameters of the Cretaceous Dunvegan Formation, Canada. Journal of Sedimentary Research 87, 97-116.

Liquete, C., Canals, M., Ludwig, W., Arnau, P., 2009. Sediment discharge of the rivers of Catalonia, NE Spain, and the influence of human impacts. Journal of Hydrology 366, 76-88.

Liu, X., Galloway, W., 1997. Quantitative determination of Tertiary sediment supply to the North Sea Basin. American Association of Petroleum Geologists Bulletin 81, 1482-1509.

Liu, Q., Zhu, X., Zeng, H., Li, S., 2019. Source-to-sink analysis in an Eocene rifted lacustrine basin margin of western Shaleitian Uplift area, offshore Bohai Bay Basin, eastern China. Marine and Petroleum Geology 107, 41-58.

Lodhia B.H., Roberts G.G., Fraser A.J., Jarvis J., Newton R., Cowan, R.J., 2019. Observation and simulation of solid sedimentary flux: examples from northwest Africa. Geochemistry, Geophysics, Geosystems 20, 4613-4634.

Lower Mississippi River Forecast Center, 2019. https://www.weather.gov/lmrfc/. Accessed 31 July 2019.

Martinsen, O.J., Sømme, T.O., Thurmond, J.B., Helland-Hansen, W., Lunt, I., 2010. Source-to-sink systems on passive margins: theory and practice with an example from the Norwegian continental margin. In: Vining, B.A., Pickering, S.C. (Eds.) Petroleum Geology: From Mature Basins to New Frontiers – Proceedings of the 7th Petroleum Geology Conference. Geological Society of London, UK, pp. 913-920.

McNeill, L.C., Shillington, D.J., Carter, G.D.O. and the Expedition 381 Participants, 2019a, Corinth Active Rift Development. Proceedings of the International Ocean Discovery Program 381. https://doi.org/10.14379/iodp.proc.381.2019

McNeill, L.C., Shillington, D.J., Carter, G.D., Everest, J.D., Gawthorpe, R.L., Miller, C., Phillips, M.P., Collier, R.E.L., Cvetkoska, A., De Gelder, G., Diz, P., 2019b. High-resolution record reveals climate-driven environmental and sedimentary changes in an active rift. Scientific Reports 9, 3116.

Meybeck, M. 1987. Global chemical weathering of surficial rocks estimated from river dissolved loads. American Journal of Science 287, 401-428.

Meybeck, M., Laroche, L., Dürr, H.H., Syvitski, J.P.M., 2003. Global variability of daily total suspended solids and their fluxes in rivers. Global and Planetary Change 39, 65-93.

Michael, N., Whittaker, A., Allen, P., 2013. The functioning of sediment routing systems using a mass balance approach: example from the Eocene of the southern Pyrenees. Journal of Geology 121, 581-606.

Michael, N.A., Carter, A., Whittaker, A.C., Allen, P.A., 2014a. Erosion rates in the source region of an ancient sediment routing system: comparison of depositional volumes with thermochronometric estimates. Journal of the Geological Society 171, 401-412.

Michael, N.A., Whittaker, A.C., Carter, A., Allen, P.A., 2014b. Volumetric budget and grain-size fractionation of a geological sediment routing system: Eocene Escanilla Formation, south-central Pyrenees. Geological Society of America Bulletin 126, 585-599.

Milliman, J.D., Meade, R.H., 1983. World-wide delivery of river sediment to the oceans. Journal of Geology 91, 1-21.

Nixon, C.W., McNeill, L.C., Bull, J.M., Bell, R.E., Gawthorpe, R.L., Henstock, T.J., Christodoulou, D., Ford, M., Taylor, B., Sakellariou, D., Ferentinos, G., 2016. Rapid spatiotemporal variations in rift structure during development of the Corinth Rift, central Greece. Tectonics 35, 1225-1248.

Nyberg, B., Helland-Hansen, W., Gawthorpe, R.L., Sandbakken, P., Eide, C.H., Sømme, T., Hadler-Jacobsen, F., Leiknes, S., 2018. Revisiting morphological relationships of modern source-to-sink segments as a first-order approach to scale ancient sedimentary systems. Sedimentary Geology 373, 111-133.

Ori, G.G., 1989. Geologic history of the extensional basin of the Gulf of Corinth (Miocene-Pleistocene), Greece. Geology 17, 918-921.

Paola, C., Martin, J.M., 2012. Mass-balance effects in depositional systems. Journal of Sedimentary Research 82, 435-450.

Parker, G., 1978. Self-formed straight rivers with equilibrium banks and mobile bed. Part 1. The sand-silt river. Journal of Fluid Mechanics 89, 109-125.

Parker, G., Paola, C., Whipple, K.X., Mohrig, D., 1998. Alluvial fans formed by channelized fluvial and sheet flow. I: Theory. Journal of Hydraulic Engineering 124, 985-995.

Parsons, A.J., Michael, N.A., Whittaker, A.C., Duller, R.A., Allen, P.A., 2012. Grain-size trends reveal the late orogenic tectonic and erosional history of the South-Central Pyrenees, Spain. Journal of the Geological Society 169, 111-114.

Pound, M.J., Salzmann, U., 2016. Heterogeneity in global vegetation and terrestrial climate change during the late Eocene to early Oligocene transition. Scientific Reports 7, 43386.

Restrepo, J., Kettner, A., Syvitski, J. 2015. Recent deforestation causes rapid increase in river sediment load in the Colombian Andes. Anthropocene 10, 13-28.

Rouby, D., Bonnet, S., Guillocheau, F., Gallagher, K., Robin, C., Biancotto, F., Dauteuil, O., Braun, J., 2009. Sediment supply to the Orange sedimentary system over the last 150 My: an evaluation from sedimentation/denudation balance. Marine and Petroleum Geology 26, 782-794.

Rowley, D.B., Garzione, C.N., 2007. Stable isotope-based paleoaltimetry. Annual Review of Earth and Planetary Science 35, 463-508.

Scheibner, C., Rasser, M.W., Mutti, M., 2007. The Camop section (Pyrenees, Spain) revisited: implications for changing benthic carbonate assemblages across the Paleocene-Eocene boundary. Paleogeography Paleoclimateology Paleoecology 248, 145-168.

Sclater, J.G., Christie, P.A., 1980. Continental stretching: an explanation of the post-Mid-Cretaceous subsidence of the central North Sea Basin. Journal of Geophysical Research: Solid Earth 85, 3711-3739.

Sharma, S., Bhattacharya, J.P., Richards, B., 2017. Source-to-sink sediment budget analysis of the Cretaceous Ferron Sandstone, Utah, USA, using the fulcrum approach. Journal of Sedimentary Research 87, 594-608.

Sheldon, N.D., Tabor, N.J., 2009. Quantitative paleoenvironmental and paleoclimatic reconstruction using paleosols. Earth-Science Reviews 95, 1-52.

Singh, A., Fienberg, K., Jerolmack, D.J., Marr, J., Foufoula-Georgiou, E., 2009. Experimental evidence for statistical scaling and intermittency in sediment transport rates. Journal of Geophysical Research: Earth Surface 114, F01025.

Strong, N., Sheets, B.A., Hickson, T.A., Paola, C., 2005. A mass-balance framework for quantifying downstream changes in fluvial architecture. In: Blum, M., Marriott, S., Leclair, S. (Eds.) Fluvial Sedimentology VII, pp. 243–253 International Association of Sedimentologists, Special Publication 35.

Syvitski, J.P.M., Milliman, J.D., 2007. Geology, geography and humans battle for dominance over the delivery of fluvial sediment to the coastal ocean. Journal of Geology 115, 1-19.

Syvitski, J.P.M., Peckham, S.D., Hilberman, R., Mudler, T., 2003. Predicting the terrestrial flux of sediment to the global ocean. Sedimentary Geology 162, 5-24.

Sømme, T.O., Helland-Hansen, W., Martinsen, O.J., Thurmond, J.B., 2009. Relationships between morphological and sedimentological parameters in source-to-sink systems: a basis for predicting semi-quantitative characteristics in subsurface systems. Basin Research 21, 361-387.

Sømme, T.O., Martinsen, O.J., Lunt, I., 2013. Linking offshore stratigraphy to onshore paleotopography: The Late Jurassic–Paleocene evolution of the south Norwegian margin. Geological Society of America Bulletin 125, 1164-1186.

Taylor, B., Weiss, J.R., Goodliffe, A.M., Sachpazi, M., Laigle, M., Hirn, A., 2011. The structures, stratigraphy and evolution of the Gulf of Corinth rift, Greece. Geophysical Journal International 185, 1189-1219.

Van Rijn, L.C., 1984. Sediment transport, part II: suspended load transport. Journal of Hydraulic Engineering 110, 1613-1641.

Walford, H.L., White, N.J., Sydow, J.C., 2005. Solid sediment load history of the Zambezi Delta. Earth and Planetary Science Letters 238, 49-63.

Watkins, S. E., 2019. Linking source and sink in an active rift : quantifying controls on sediment export and depositional stratigraphy in the Gulf of Corinth, central Greece. PhD thesis, Imperial College London, 245 p. DOI: https://doi.org/10.25560/68579.

Watkins, S.E., Whittaker, A.C., Bell, R.E., McNeill, L.C., Gawthorpe, R.L., Brooke, S.A., Nixon, C.W., 2019. Are landscapes buffered to high-frequency climate change? A comparison of sediment fluxes and depositional volumes in the Corinth Rift, central Greece, over the past 130 ky. Geological Society of America Bulletin 131, 372-388.

Watkins, S.E., Whittaker, A.C., Bell, R.E., Brooke, S.A., Ganti, V., Gawthorpe, R.L., McNeill, L.C., Nixon, C.W., 2020. Straight from the source's mouth: controls on field-constrained sediment export across the entire active Corinth rift, central Greece. Basin Research, DOI: 10.1111/bre.12444.

Weight, R.W., Anderson, J.B., Fernandez, R., 2011. Rapid mud accumulation on the central Texas shelf linked to climate change and sea-level rise. Journal of Sedimentary Research 81, 743-764.

Whitchurch, A.L., Carter, A., Sinclair, H.D., Duller, R.A., Whittaker, A.C., Allen, P.A., 2011. Sediment routing system evolution within a diachronously uplifting orogen: insights from detrital zircon thermochrinological analyses from the south-central Pyrenees. American Journal of Science 311, 442-482.

Whittaker, A.C., Duller, R.A., Springett, J., Smithells, R.A., Whitchurch, A.L., Allen, P.A., 2011. Decoding downstream trends in stratigraphic grain size as a function of tectonic subsidence and sediment supply. Geological Society of America Bulletin 123, 1363-1382.

Wolfe, J.A., 1995. Paleoclimatic estimates from Tertiary leaf assemblages. Annual Review of Earth and Planetary Sciences 23, 119-142.

Zachos, J., Pagani, M., Sloan, L., Thomas, E., Billups, K., 2001. Trends, rhythms, and aberrations in global climate 65 Ma to present. Science 292, 686-693.

Zachos, J.C., Dickens, G.R., Zeebe, R.E., 2008. An early Cenozoic perspective on greenhouse warming and carbon-cycle dynamics. Nature 451, 279-283.

Zhang, J., Covault, J., Pyrcz, M., Sharman, G., Carvajal, C., Milliken, K., 2018. Quantifying sediment supply to continental margins: application to the Paleogene Wilcox Group, Gulf of Mexico. American Association of Petroleum Geologists Bulletin 102, 1685-1702.

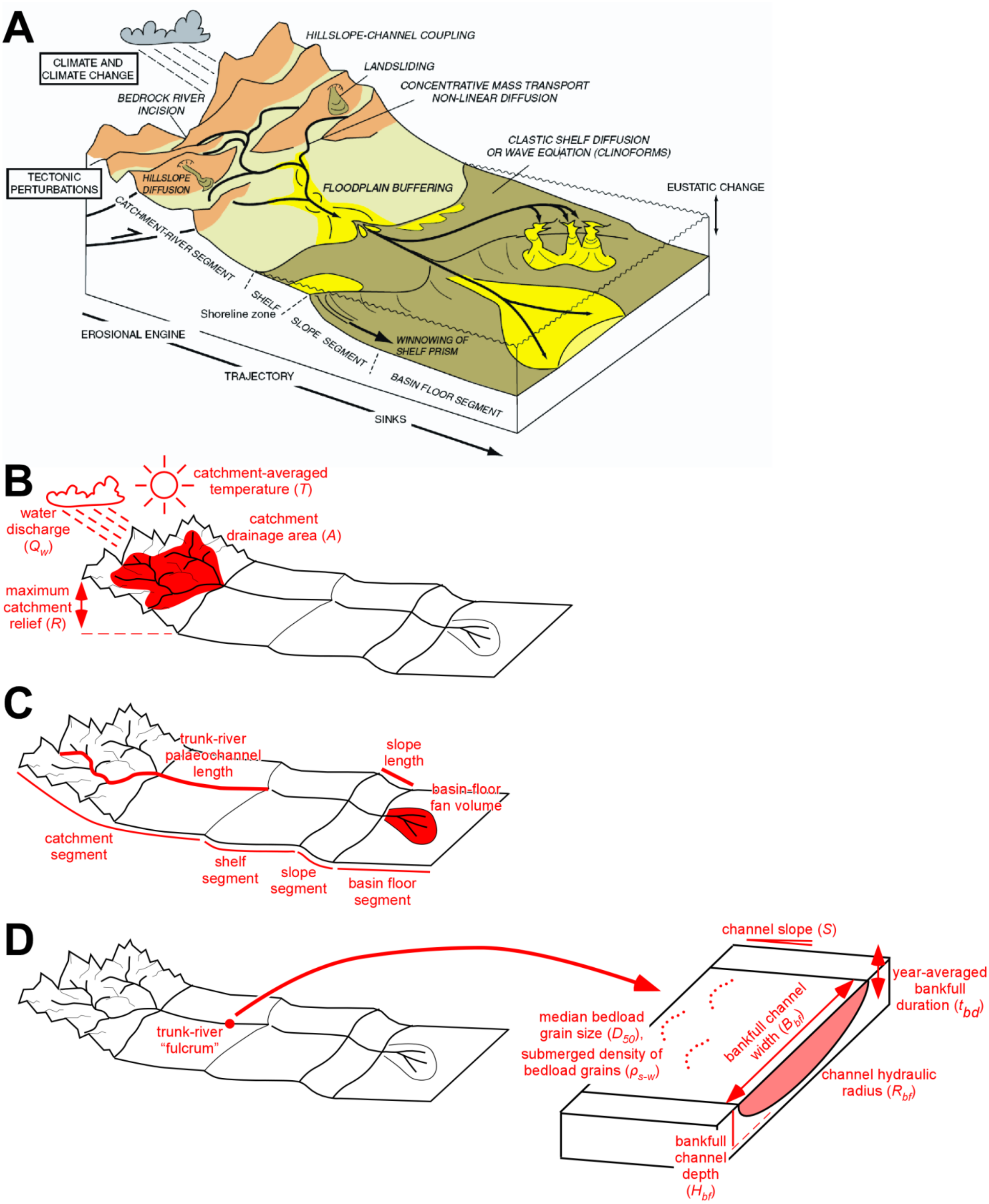

Figure 1. (**A**) Conceptual model of the sediment routing system, from net-erosional source to net-depositional sink (Allen and Heller 2011, their figure 6.2). (**B-D**) Simplified versions of the conceptual model highlighting key parameters in red used to estimate sediment flux in sediment routing systems (Table 1) using: (**B**) the BQART model (Syvitski and Milliman, 2007); (**C**) geomorphological scaling relationships (Sømme et al., 2009); and (**D**) the 'fulcrum' model (Holbrook and Wanas, 2014).

Parameter	**BQART model**	**Geomorphological scaling relationships**	**"Fulcrum" model**
catchment drainage area (*A*)	x	x	
maximum catchment relief (*R*)	x		
catchment-averaged temperature (*T*)	x		
catchment-averaged lithology (*L*)	x		
glacial erosion factor (*I*)	x		
trapping efficiency of lakes and reservoirs (T_E)	x		
human-influenced soil erosion factor (E_H)	x		
water discharge (Q_w)	x		
fluvial-palaeochannel length		x	
slope length		x	
basin-floor fan volume		x	
duration of deposition, derived from age model		x	
fluvial-palaeochannel averaged bankfull depth (H_{bf})			x
fluvial-palaeochannel bankfull width (B_{bf})			x
palaeochannel hydraulic radius (R_{bf})			x
median bedload grain size (D_{50})			x
submerged density of bedload grains (ρ_{s-w})			x
bankfull Shields number for dimensionless shear stress (τ^*_{bf50})			x
fluvial-palaeochannel slope (*S*)		x	x
year-averaged bankfull duration (t_{bd})			x

Table 1. Parameters for which input data are potentially required for each sediment-flux estimation method. Different combinations of geomorphological scaling relationships, which thus require different input parameters, can be used to estimate sediment flux. Fluvial-palaeochannel bankfull width (B_{bf}) and averaged bankfull depth (H_{bf}) are used to estimate hydraulic radius (R_{bf}). Some combinations of B_{bf} and H_{bf} are inconsistent with input data; R_{bf} is used as a filtering parameter to remove such combinations.

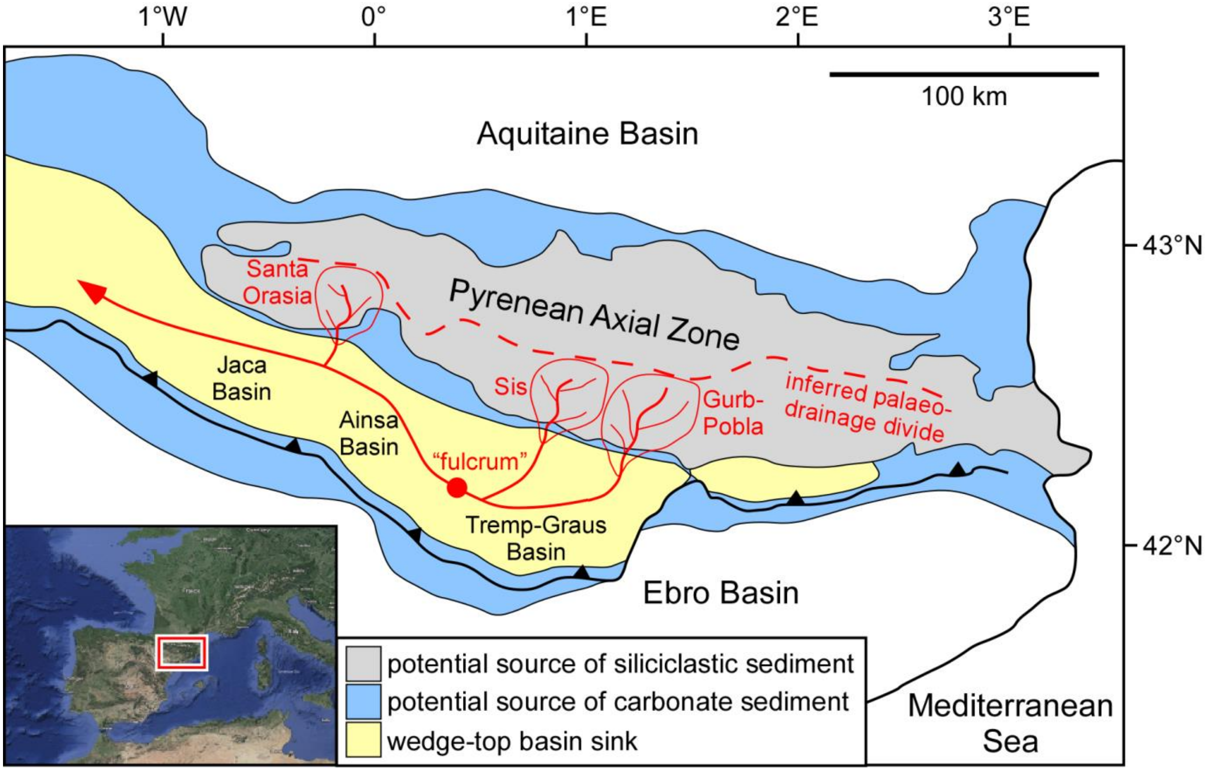

Figure 2. Location of the Late Eocene Escanilla sediment routing system in the wedge top (Tremp-Graus, Ainsa and Jaca basins) of the South Pyrenean Foreland Basin system. Three transverse catchments (Gurb-Pobla, Sis and Santa Orasia) developed in the Pyrenean Axial Zone, and formed source areas for the axial Escanilla sediment routing system (shown in red). The positions of the trunk river and intra-catchment drainage networks are shown schematically. The "fulcrum" (red dot) shows the study area of Labourdette (2011), where channelised sandbodies representative of the trunk river were characterised. The inset map shows the present-day position of Escanilla sediment routing system deposits using Google Earth satellite imagery.

Parameter	**BQART model**	**Geomorphological scaling relationships**	**"Fulcrum" model**
catchment drainage area (*A*)	4-19 x 10^3 km^2	not required	
maximum catchment relief (*R*)	1-5 km		
catchment-averaged temperature (*T*)	19-25 °C		
catchment-averaged lithology (*L*)	1		
glacial erosion factor (*I*)	1		
trapping efficiency of lakes and reservoirs (T_E)	0		
human-influenced soil erosion factor (E_H)	1		
water discharge (Q_w)	1.0-6.4 m^3/s		
fluvial-palaeochannel length		80-140 km	
slope length		scaled from fluvial-palaeochannel length	
basin-floor fan volume		scaled from slope length	
duration of deposition, derived from age model		2.6 Myr	
fluvial-palaeochannel averaged bankfull depth (H_{bf})			3-20 m
fluvial-palaeochannel bankfull width (B_{bf})			40-390 m
palaeochannel hydraulic radius (R_{bf})			2.5-17.9 m
median bedload grain size (D_{50})			0.4-0.8 mm
submerged density of bedload grains (ρ_{s-w})			1.60-1.70
bankfull Shields number for dimensionless shear stress (τ^*_{bf50})			1.86
fluvial-palaeochannel slope (*S*)		not required	calculated from H_{bf}, D_{50}, *R*, τ^*_{bf50}
year-averaged bankfull duration (t_{bd})			0.1-120 days/yr

Table 2. Parameter values used to estimate sediment flux in the Escanilla sediment routing system (Fig. 2).

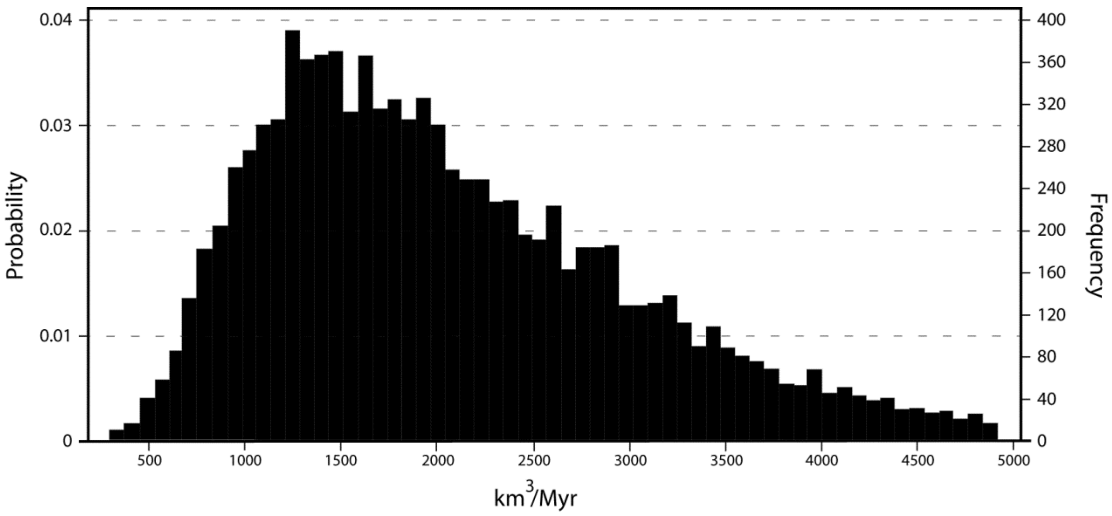

Figure 3. Probability distribution of sediment-flux estimates for the Escanilla sediment routing system generated using 10,000 Monte Carlo simulated realisations of the BQART model (Equations 1, 2), input parameter-value ranges listed in Table 2, and associated parameter-value distributions (see section 3.2 for details). The distribution shows 9872 realisations that lie within the mean value of sediment flux ± 8 standard deviations.

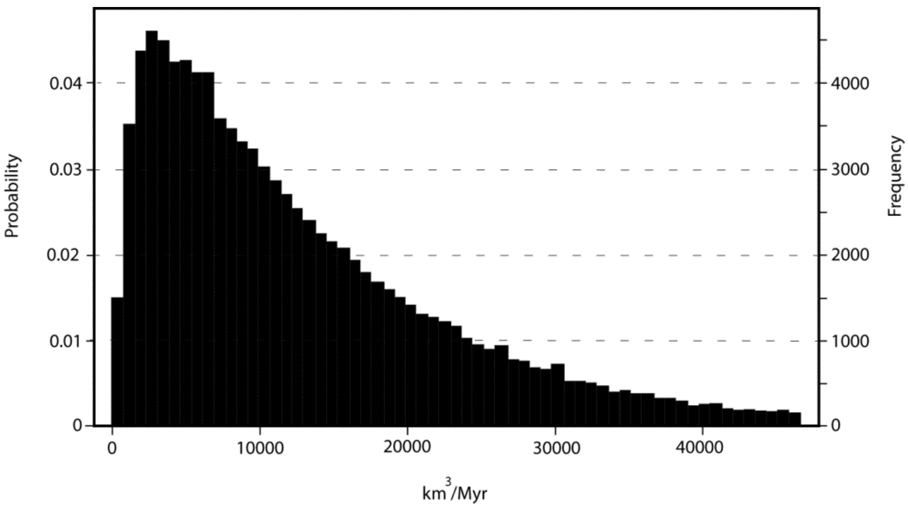

Figure 4. Probability distribution of sediment-flux estimates for the Escanilla sediment routing system generated using 10,000 Monte Carlo simulated realisations of the "fulcrum" model (Equations 4-9), input parameter-value ranges listed in Table 2, and associated parameter-value distributions (see section 3.4 for details). The distribution shows 9840 realisations that lie within the mean value of sediment flux ± 8 standard deviations.

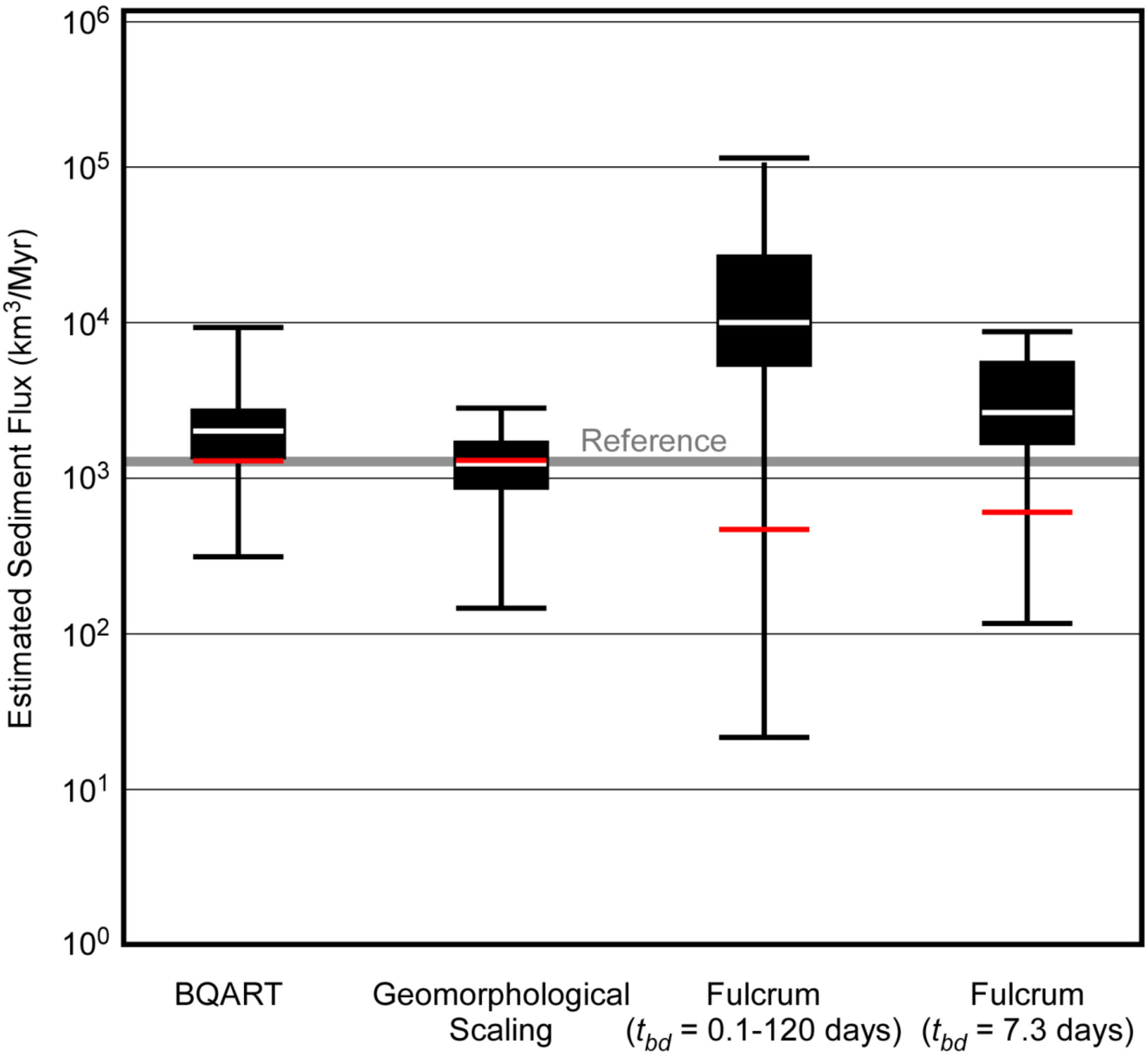

Figure 5. Box-and-whisker plots of sediment flux for the Escanilla sediment routing system (Fig. 2) generated by the BQART model, geomorphological scaling relationships, and "fulcrum" model estimation methods, compared to reference value of decompacted sediment accumulation rate based on mapped, dated sediment volumes. Each box-and-whisker plot shows the base-case value (red horizontal line; defined by the modal value of each input parameter), median value (white horizontal line), interquartile range (black box) and full range (defined by whiskers). Where the base-case value lies outside of the interquartile range, this arises from strong skew in the distribution of values assigned to one or more input parameters. Note that sediment flux is shown with a logarithmic scale.

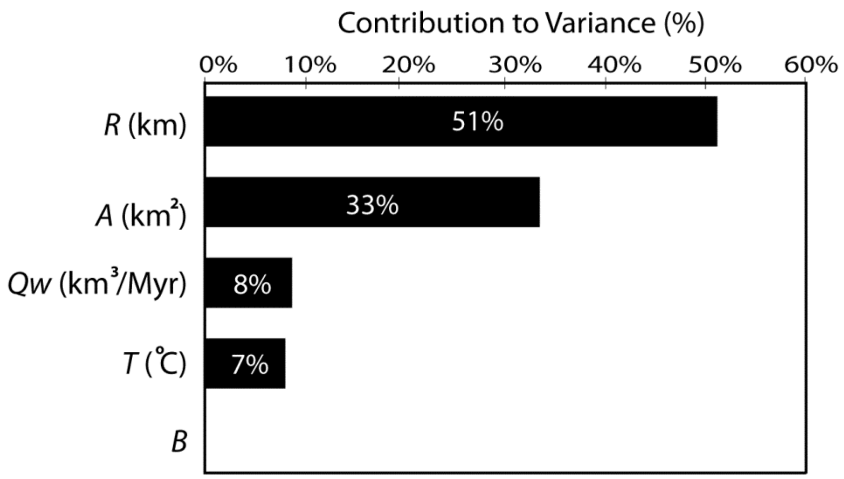

Figure 6. Plot showing the sensitivity of sediment-flux estimates for the Escanilla sediment routing system to input parameters of the BQART model. The plot uses 10,000 Monte Carlo simulated realisations of the BQART model (Equations 1, 2), input parameter-value ranges listed in Table 2, and associated parameter-value distributions (see section 3.2 for details).

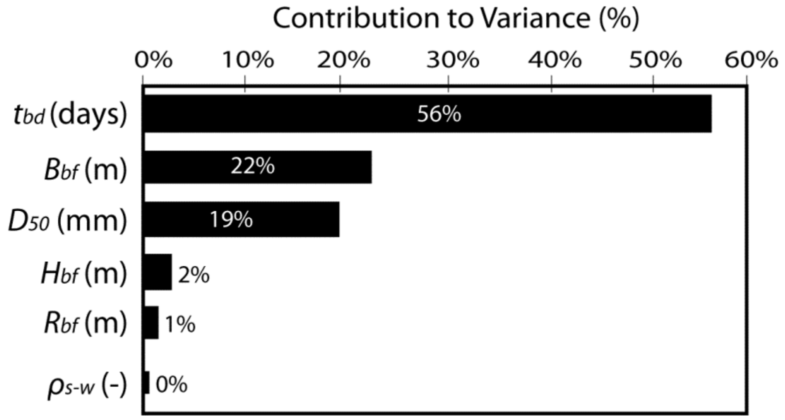

Figure 7. Plot showing the sensitivity of sediment-flux estimates for the Escanilla sediment routing system to input parameters of the "fulcrum" model. The plot uses 10,000 Monte Carlo simulated realisations of the "fulcrum" model (Fig. 4), based on the range of-values (Table 2) and distributions (section 3.4) assigned to these parameters.

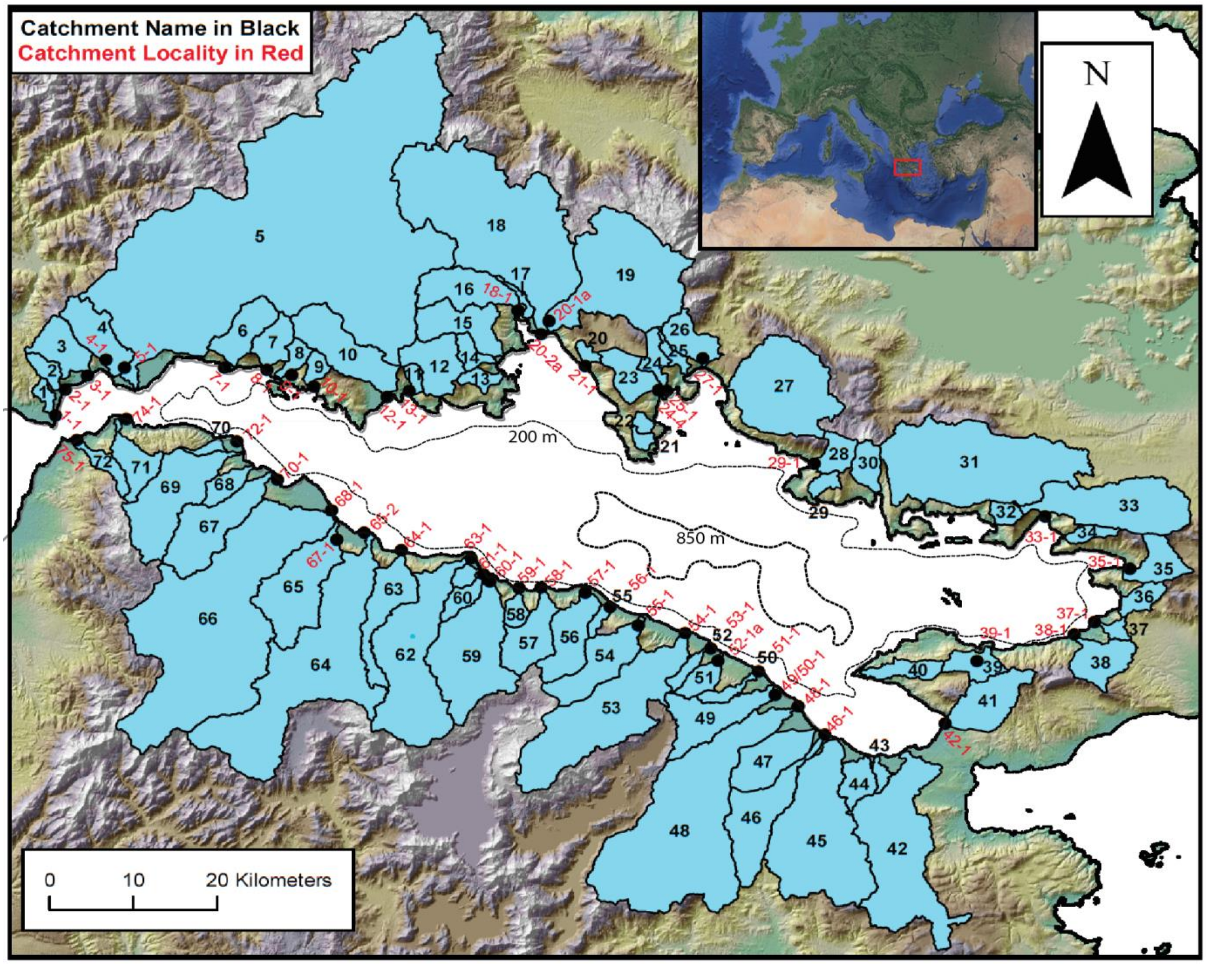

Figure 8. Location of the modern Gulf of Corinth Rift Basin, Greece and the 73 relatively large (catchment area >5 km^2) sediment routing systems that drain into the closed Gulf of Corinth depocentre (after Watkins et al., 2019). The 200 m and 850 m depth contours within the Gulf are shown.

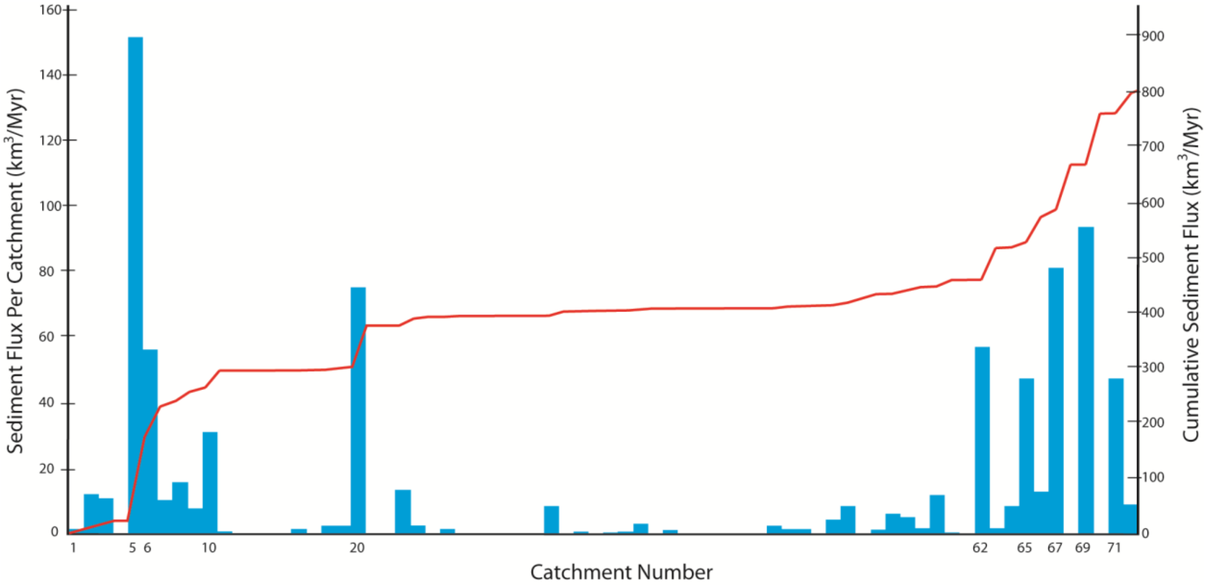

Figure 9. Sediment flux estimated for each catchment in the Gulf of Corinth Rift Basin (Fig. 8) using the "fulcrum" model and data from Watkins (2019). Catchments are numbered as in Figure 8, but for clarity only numbers for selected catchments (with sediment flux >20 km^3/Myr) are shown. Data are plotted as sediment flux for individual catchments (blue bars) and as cumulative sediment flux (red line). Sediment flux is dominated by the contributions from a few catchments.

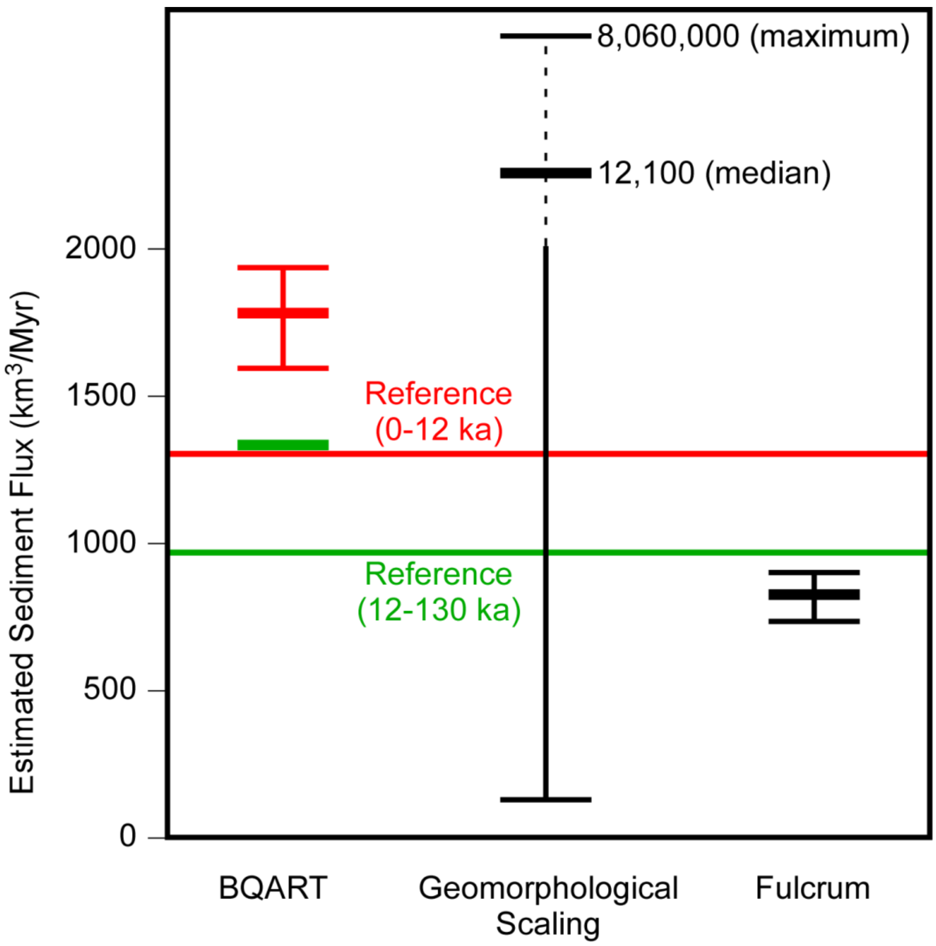

Figure 10. Box-and-whisker plots of sediment-flux ranges for sediment routing systems in the Gulf of Corinth Rift Basin (Fig. 8) generated by the BQART model, geomorphological scaling relationships, and "fulcrum" model estimation methods, compared to reference value of decompacted sediment accumulation rate based on mapped, dated sediment volumes. Each box-and-whisker plot shows the median value (horizontal line) and full range (defined by whiskers). Note that sediment flux is shown with a linear scale, but the median and maximum values of sediment flux for the geomorphological scaling relationships are not shown to scale. Reference values and estimates generated by the BQART model are shown for two time intervals (0-12 ka in red and 12-130 ka in green, both with small range), whereas estimates for the geomorphological scaling relationships and "fulcrum" model are shown for a single time interval (0-130 ka).

Method	**0-12 ka**	**12-130 ka**
Reference: seismically mapped volume (km^3)	16	114
BQART model: estimated volume (km^3)	21	159
Geomorphological scaling relationships: estimated volume (km^3)	150	1400
"Fulcrum" model: estimated volume (km^3)	10	108

Table 3. Sediment volumes for sediment routing systems in the Gulf of Corinth Rift Basin (Fig. 8) generated by the BQART model, geomorphological scaling relationships, and "fulcrum" model estimation methods, compared to reference values of decompacted, mapped sediment volumes (Watkins et al., 2019). Median volumes are reported for time intervals 0-12 ka and 12-130 ka.